The slow downwearing of Madagascar: inferring patterns and controls on long-term basin-averaged erosion rates from *in-situ* ^{10}Be at the catchment and regional level

Abstract

Cosmogenic nuclide analysis of river sediment provides insight into catchment-wide erosion rates and dynamics. Here, we investigate spatial patterns and controls on ^{10}Be-inferred erosion rates in Madagascar, a moderately seismically active microcontinent surrounded by passive margins with locally steep topography and a climate that varies from humid tropical to semi-arid. We use a compiled dataset of 99 detrital ^{10}Be measurements, 63 of which are new, covering more than 30% of the country and a wide range of topographic, bioclimatic and geologic characteristics. Overall, ^{10}Be erosion rates are low (2.4 - 51.1 mm kyr^{-1}), with clear differences between regions. The lowest rates are measured on the central highlands (~8 mm kyr^{-1}), in the Alaotra-Ankay graben (~11 mm kyr^{-1}), and in the large north-central catchments (~11 mm kyr^{-1}). Higher rates are found on the steep eastern escarpment (~20 mm kyr^{-1}), in the northwest (~31 mm kyr^{-1}), and in the southwest (~29 mm kyr^{-1}). A stepwise linear regression model identified elevation as the main factor associated with variations in ^{10}Be erosion rates (lower rates for higher catchments). Random within-between statistical models (REWB), on the other hand, indicated that the differences between different regions can be explained by differences in river concavity, seismic events, and gully (lavaka) densities, whereas additional variation within regions is only linked to seismicity. We find no correlation between catchment or river steepness and ^{10}Be-inferred erosion rates. Our results indicate that in Madagascar long-term erosion rates are overall low, and that simple topography-based models do not explain variations in rates of landscape change inferred from ^{10}Be concentrations in river sediment. We demonstrate that identifying different regions aids in interpreting spatial patterns of erosion rates, and that REWB models can be a powerful tool in deciphering environmental controls on ^{10}Be erosion rates.

This article has been accepted for publication and undergone full peer review but has not been through the copyediting, typesetting, pagination and proofreading process which may lead to differences between this version and the Version of Record. Please cite this article as doi: 10.1002/esp.5586

Keywords: Madagascar, detrital CRN, long-term erosion rates, random-within between models, *in-situ* ^{10}Be

1 Introduction

Cosmogenic radionuclides (CRNs) in river sediments are a valuable tool to determine spatially averaged erosion rates, offering a window on long-term (1 000 - 1 000 000 yr) landscape dynamics. River sands integrate across the drainage basin, and CRN concentrations average out the episodic nature of sediment supply, providing an estimate of the long-term background erosion rates (von Blanckenburg, 2005; Dunai, 2010; Vanacker et al., 2007b; Bierman and Steig, 1996). Landscapes where the parent material is overlain by a thick and intensively weathered layer, the regolith, cover large parts of the Earth's surface and are prone to rapid geomorphic response to land use change (Winkler et al., 2021; Song et al., 2018; Brosens et al., 2022a). Especially in these settings, information on background erosion rates and their controls is crucial if the impact of these changes on landscape dynamics and how they might have evolved over time is to be understood (Vanacker et al., 2007a; Bartley et al., 2015; Hewawasam et al., 2003).

Madagascar is a microcontinent with locally steep topography and active seismicity despite being surrounded by passive margins (de Wit, 2003; Rakotondraibe et al., 2020). Low ^{10}Be erosion rates between 4 and 34 mm kyr^{-1} have been reported (Cox et al., 2009; Wang et al., 2021) for the central and eastern parts of Madagascar, which integrate over timescales of $\sim$ 30 to 250 kyr (the time it takes to erode the upper 1.0 m of soil (von Blanckenburg, 2005)). These rates can be considered a robust estimate of pre-anthropogenic erosion rates for these regions, as substantial human populations have existed on the island for only a few thousand years (Douglass et al., 2019; Hansford et al., 2018). Madagascar is large and diverse with distinct regions differing in geology, geomorphology, climate and ecology that vary from tropical forest in the east over temperate highlands in the center to semi-arid regions in the southwest (Tyson, 2013; de Wit, 2003). To better constrain and understand the magnitude, spatial patterns and environmental controls of pre-anthropogenic erosion rates across the varied regions of Madagascar we focus on two main research questions: i) is there a systematic spatial pattern in variation in ^{10}Be erosion rates in Madagascar?, and ii) if so, which environmental variables explain variation in island-wide ^{10}Be erosion rates?

We investigated these questions by applying various statistical analyses to a suite of 99 *in-situ* ^{10}Be concentrations from river sediment. This dataset, which combines published data (Cox et al., 2009; Wang et al., 2021) with 63 new samples, covers about 30% of Madagascar's land mass and therefore allowed us to study if environmental variables can explain variations in ^{10}Be-erosion rates in Madagascar and to consider both differences between individual catchments and differences between the different regions.

2 Madagascar's diversity

Eastern Gondwana (Madagascar, India, Sri Lanka, Antarctica and Australia) separated from what is now the African continent 165 - 155 Ma years ago and continued rifting led to the break-up of Madagascar and India 120 - 84 Ma years ago (Reeves et al., 2002; Collins and Windley, 2002; Gibbons et al., 2013; Eagles and Hoang, 2014; de Wit, 2003). Two thirds of Madagascar's surface (center and east) is underlain by Precambrian crystalline basement, while Cenozoic sedimentary formations are mostly found in the western part. Cretaceous and Neogene volcanic deposits can be found across the island (de Wit, 2003) (Figure 1c). Madagascar is a microcontinent that spans 13° of latitude and is bounded by passive margins (de Wit, 2003) (Figure 1a). The topography is strongly asymmetric, rising from sea level to > 1 000 m over a distance of only 50 km across the eastern escarpment, whereas in the west the topography more gently dips into the Mozambique Channel (Battistini, 1972) (Figure 1b). Elevation of the central highlands peaks up to 2700 m, likely resulting from topographic rejuvenation and renewed denudation after regional uplift during the Oligo-Miocene (Stephenson et al., 2021). The highlands are characterized by a rolling relief with steep convex hillslopes that are covered by a thick layer of regolith; and despite the fact that friable saprolites extend more than 10 m and in places up to 100 m deep, they hold up steep slopes that are locally > 40° (Battistini, 1972). There is active tectonic rifting in the Alaotra-Ankay graben (AAG) and seismic activity with earthquakes of magnitude 0.5 - 5.6 is clustered around the graben, as well as on the Itasy and Ankaratra volcanic fields (Cox et al., 2010; de Wit, 2003; Rakotondraibe et al., 2020) (Figure 1 g,h). In many parts of the highlands, large, steep-sided gullies called 'lavaka' have cut deeply into the regolith, the relative abundance of which spatially correlates with seismic activity (Kusky et al., 2010; Cox et al., 2010).

The combination of these large topographic variations and a significant latitudinal extent results in a wide range of climatic and biogeographical conditions. There are two prominent rainfall gradients across the island: a strong east to west rainfall falloff with distance from the eastern escarpment, and a more muted north to south decrease related to latitudinal climate regions (Donque, 1972; Nassor and Jury, 1998; Cornet, 1974) (Figure 1e). These variations are reflected in the different vegetation types, with humid forests in the east, dry deciduous forest in the west, succulent woodlands in the southwest, spiny desert vegetation in the south and subhumid forest and open grasslands in the central highlands (Figure 1d,f) (Koechlin et al., 1972; Burgess et al., 2004).

3 Methods

3.1 CRN-derived erosion rates

A dataset containing 99 *in-situ* ^{10}Be measurements from river sediment samples was compiled. The catchments in the dataset represent 30% of surface area of

Madagascar (Table S1). 63 of the datapoints are new data which we combine with previously published data from the eastern escarpment and central highlands (Cox et al., 2009; Wang et al., 2021) (Figure S1). Additionally, 4 river terrace sediments were sampled and analyzed for *in-situ* ^{10}Be concentrations.

3.1.1 River sediment samples

The sampled catchment areas range from 1 to 37 000 km^2 and have a mean and median area of 2400 km^2 and 400 km^2, respectively (Table S1, Figure 2). The majority of the samples come from the central highlands (n = 27) and the eastern escarpment (n = 32). 12 catchments are located within the Alaotra-Ankay graben system, and 11 samples come from smaller catchments in the southwest. Only a limited number of measurements is available for the eastern plain (n = 1), and northwest Madagascar (n = 5). The largest sampled catchments (> 10 000 km^2) are located in the north-central (n = 4) and south-western (n = 2) part of the island; a number of smaller sampled catchments are nested within these largest catchments (see Table S1, Figure S2 and Figure S3).

In-situ ^{10}Be concentrations give an indication of the total denudation (physical erosion and chemical weathering) of the upper meters of regolith, but do not reflect fluxes related to deep chemical weathering beneath the cosmic ray attenuation depth (Riebe and Granger, 2013; Dixon et al., 2009; von Blanckenburg, 2005; Bierman and Steig, 1996). These deep fluxes can be considerable in tropical regoliths (Riebe and Granger, 2013; Dixon et al., 2009; Campbell et al., 2022), such as are found in Madagascar. We therefore refer to "^{10}Be erosion rates" throughout this work to make it explicit that our data do not account for potential mass loss by dissolution deep within the regolith.

Cosmogenic nuclide-derived erosion rates were calculated from the measured concentrations of *in-situ* produced ^{10}Be in quartz of submerged river sediment. All river sediment samples were collected midstream from active river channels. Wang et al. (2021) amalgamated samples from 200-500 m reaches along the channel, where the 125-500 μm fractions were used for quartz purification. All other river sediment samples were collected at one location, where the 250-841 μm fraction was used for analysis. For all samples, the ^{10}Be was extracted from purified quartz grains using standard methods as described in von Blanckenburg (2004), Kohl and Nishiizumi (1992), Corbett et al. (2016) and Vanacker et al. (2007b). ^{10}Be/^{9}Be ratios were measured in BeO targets with accelerator mass spectrometry (AMS) (see Text S1.1 for details). The measured ^{10}Be concentrations were corrected using laboratory blanks. Uncertainties include analytical AMS and propagated blank errors. Catchment-averaged erosion rates were calculated from the ^{10}Be concentrations using the CAIRN method of Mudd et al. (2016), where all samples were reprocessed using the same procedure to allow comparison (see text S1.2 for details). Comparison of the ^{10}Be concentrations of four (partially) overlapping catchments from the different data sources shows that the measured ^{10}Be concentrations agree within the total uncertainty (AMS + laboratory blanks), suggesting that the slight differences in sampling and processing protocols have no measurable effect on the reported ^{10}Be concentrations (Figure S4).

The nested catchment structure was taken into account by following the approach of Portenga et al. (2015) and Granger et al. (1996). When the area of the sub-catchment is > 20% of the main catchment, an effective erosion rate (EER) was calculated for that part of the main catchment outside of the sub-basin, based on the calculated erosion rate (E) and area (A) of the main catchment and sub-basin (see inset Figure S2 for used nomenclature). The erosion rate for the main catchment was then substituted by EER:

$$EER = \frac{A_{main}E_{main} - A_{subbasin}E_{subbasin}}{A_{main} - A_{subbasin}} \quad (1)$$

when the area of the sub-catchment was < 20% of the main catchment, no effective erosion rate was calculated for the sub-basin and only the erosion rate of the main catchment was used (Table S1).

3.1.2 Terrace samples

For four rivers additional terrace samples were collected and analyzed for *in-situ* ^{10}Be concentrations. Comparing these values with those observed for the present river sediments gives an indication whether there have been significant changes in basin-wide erosion rates over the time scales covered by terrace formation (Cox et al., 2009) (Table S1). Terrace samples represent well-sorted traction-structured fluvial sands (exhibiting either large-scale cross-bedding or flat lamination) exposed in the cutbanks of incising rivers, and were chosen if they were i) buried beneath at least one soil horizon greater than 1 m thick (indicating at minimum several centuries of residence time); and ii) contained charcoal (twigs and small woody chunks) clearly contemporaneous with the sediment (i.e. not associated with modern roots or other disturbances, and deposited along cross-sets or internal laminations). Samples were sieved in the field to extract the medium and coarse sand fractions (250-841 μm), after which they were processed for ^{10}Be following the same procedure as the river sediment samples (see section 3.1.1). The charcoal contained in the terrace samples was dated using ^{14}C analyses by Beta Analytic and were calibrated according to Reimer et al. (2004) using INTCAL04.

3.2 Environmental variables

We considered fifteen variables that might explain variations in ^{10}Be erosion rates, encompassing various topographic, river, geological, bioclimatic and geomorphological indicators: i) catchment area, ii) elevation, iii) slope, iv) roughness, v) relief, vi) normalized river steepness, vii) stream concavity index, viii) concavity θ of all rivers and the ix) trunk river (θ_t), x) lithological erodibility (LE), xi) seismic events, xii) peak ground acceleration (PGA), xiii) precipitation, xiv) bioclimate, and xv) lavaka density.

Catchment topography

Topographic analyses, catchment delineation, and river extraction were performed on the carved and filled 30 m SRTM DEM (Farr et al., 2007) using TopoToolbox 2 (Schwanghart and Scherler, 2014). The DEM was projected to UTM38S coordinates (EPSG: 32738). We calculated four topographic variables for each catchment: the mean elevation [m], mean slope gradient [°], mean roughness [-], and catchment relief [m]. Catchment elevation gives a first indication of the topographic setting of a catchment (lowland vs. highland) and will in part also reflect variations in precipitation and vegetation. Slope gradient was calculated using an 8-connected neighborhood algorithm, and terrain roughness as the largest difference between the central pixel and its surrounding pixels using a kernel size of 3 $\times$ 3 (Schwanghart and Scherler, 2014). Catchment relief is the difference in elevation between the highest and lowest point of the catchment.

River characteristics

We extracted the river network using a channel initiation threshold of 0.5 km² following Campforts et al. (2020). The stream power law is widely used to model bedrock channel incision, and can be formulated in its simplest form as:

$$E = KA^m S^n \quad (2)$$

where E is the long-term erosion rate, K an erodibility coefficient that encompasses e.g. climate and lithology, A the upstream drainage area (as an indicator for discharge), S the channel slope, and m and n exponents determined by the fluvial processes (Howard, 1994; Lague, 2014). Flint's law (Flint, 1974) states that the channel slope of rivers varies as an inverse power law to the drainage area:

$$S = k_s A^{-\theta} \quad (3)$$

where k_s is the river profile steepness and $\theta = m/n$, the concavity of the river profile (Snyder et al., 2000; Whipple and Tucker, 1999). Equation (2) can then be rewritten as a function of k_s:

$$E = Kk_s^n \tag{4}$$

We performed a χ-analysis on the entire river network of Madagascar with a baselevel of 0 m (chiplot algorithm, Schwanghart and Scherler, 2014) from which θ-values for the individual catchments were derived, both when considering all rivers in the catchment and when considering only the trunk stream (θ_t). The mean θ-value of all drainage basins was equal to 0.42. As this value is close to the theoretical value of 0.45, we calculated the normalized channel steepness, k_{sn}, using a fixed θ of 0.45 in order to allow comparison between the different catchments (Wobus et al., 2006; Whipple, 2004). k_{sn} was then calculated for the entire river network and averaged per drainage basin.

Additionally, we used the stream concavity index (SCI) to calculate the concavity of the river profiles from the normalized and smoothed river longitudinal profiles of the trunk streams (Zaprowski et al., 2005; Demoulin, 1998). SCI ranges between -1 and 1, where positive values are indicative for concave profiles and negative values are equivalent to convex river profiles (Zaprowski et al., 2005).

Lithology and seismic activity

We estimated average catchment values for three geological metrics: i) lithological erodibility of the parent material (LE, [-]), ii) seismic event frequency [events km^{-2}], and iii) peak ground acceleration (PGA [g]). We calculated the LE following the approach of Campforts et al. (2020) by combining information on rock composition (Aalto et al., 2006) and the stratigraphic age of non-igneous formations (Kober et al., 2015):

$$LE = \frac{2}{7}L' \tag{5}$$

where L' differs depending on whether the geology is dominated by igneous or non-igneous rocks, thus:

$$L' = \begin{cases} \frac{L_A + L_L}{3}, & \text{non-igneous rocks} \\ \frac{L_L}{2}, & \text{igneous rocks} \end{cases} \quad (6)$$

L_A is a dimensionless erodibility index based on stratigraphic age (Table S2) and L_L is a dimensionless erodibility index based on lithological strength (Table S3). We obtained the bedrock lithology from the 1/1 000 000 geological map of Madagascar (Roig et al., 2012; Tucker et al., 2014) based on which we calculated LE. It is important to acknowledge that the LE is calculated for the underlying parent material. In the central highlands, the bedrock is typically covered by a thick laterized regolith and also elsewhere the rivers might be incising into regolith instead of bedrock. As we miss accurate information on spatial variations in the thickness of the regolith cover in Madagascar we did not further quantify this.

Madagascar has a continental passive margin setting, but is a seismically active landmass due to rifting. We therefore considered both the number of seismic events and modeled peak ground acceleration (PGA, [g]). We used a catalogue of 3442 seismic events (magnitudes 0.5-5.6), recorded between 1979 and 1994 (Ramanantsoa, 2000) and in 1996 (Institut et Observatoire de Géophysique D'Antananarivo, 2008), which were geospatially analysed by Cox et al. (2010), who produced a seismic event density map of Madagascar. This provides a robust sampling of Malagasy seismicity which is considered to be representative of longer-term seismic activity as it is aligns with tectonic features and the more recent seismic catalog of Rakotondraibe et al. (2020) which is, however, only based on 23-months of deployment and 692 events, making it less statistically valid for our purpose. The PGA data were obtained from the Sub-Saharan Africa (SSA) Earthquake Model (Poggi et al., 2017).

Bioclimate

We also considered climatic and vegetation regimes in Madagascar using two bioclimatic variables: i) precipitation and iii) bioclimatic region. We calculated mean annual precipitation over the period 1981 - 2020 from CHIRPS, which is a gridded 0.05° $\times$ 0.05° precipitation product derived from satellite imagery and station data (Funk et al., 2014). As our CRN data integrate over tens to hundreds of thousands of years (30 - 250 kyr) absolute precipitation amounts will have fluctuated over the considered time period. Bayesian modelling of Plio-Pleistocene climate transitions in Africa from terrigenous dust records enabled the identification of multiple dominant transition events, where the most recent event took place around 700 - 600 kyr ago, thereby predating our longest integration period (Kukla, 2005). However, the longest integration times (up to 250 kyr) cover one to two glacial-interglacial cycles (Kukla, 2005) during which large wet and dry extremes occurred (Kutzbach et al., 2020). Also the shorter integration times include periods of climatic variation, where the last glacial maximum (19 - 23 kyr BP) was generally dryer and where wetter conditions prevailed during the Younger Dryas (11.5-12.8 kyr BP) in Eastern Africa (Garcin et al., 2006). Thus, absolute precipitation amounts will have fluctuated over the CRN integration time: by using present values we implicitly assume that the present spatial pattern is representative for the entire integration period.

There are clear indications that the vegetation cover of Madagascar has undergone drastic changes over the past millennium with a general decline in forest cover that has been linked to anthropogenic impacts (Joseph and Seymour, 2020; Joseph et al., 2021; McConnell and Kull, 2014; Reinhardt et al., 2022; Gasse and Van Campo, 2001). We therefore did not include the current forest cover as an environmental variable, but work with generalized bioclimatic regions. We delineated five simplified bioclimatic regions based on Cornet (1974) and Crowley (2010) and assigned a number from 1 (moist and densely vegetated) to 5 (dry with only sparse vegetation cover) reflecting both differences in precipitation and vegetation density: 1 = humid forest, 2 = central highlands, 3 = dry deciduous forest, 4 = succulent woodland, 5 = spiny thicket (Figure 1d). Coupled paleoclimate-vegetation models show that vegetation patterns have shifted in response to climatic variations, with modelled changes in the grassland and forest extent in Madagascar over the past 140 kyr (Kutzbach et al., 2020). Again, we consider these regions as relative rather than absolute patterns.

Geomorphology

We obtained lavaka densities [lavaka km^{-2}] for 88 of our 99 catchments (up to a maximum size of 11 000 km²) by direct counting from Google Earth imagery at eye altitude of 2.5 km (corresponding to 1/7500 scale). These 0.5 m resolution images permitted identification of active lavaka with a width as small as 10 m. For four catchments (id = 99, 96, 26 and 29, Table S4) we used previously published counts from Voarintsoa et al. (2012). For the seven largest catchments (12 000 - 37 000 km², Table S4) we used a rating curve based on comparison between our counts and those of Cox et al. (2009) that were derived from sharpened Landsat ETM+ (15 m resolution) imagery. Estimates from the coarser resolution ETM+ imagery are systematically lower than the higher resolution Google Earth estimates and were therefore recalculated using a rating curve (Figure S5).

We subdivided the catchments into 8 different classes based on size and region: i) central highlands (n = 27), ii) Alaotra-Ankay graben (AAG, n = 12), iii) eastern escarpment (n = 32), iv) eastern plain (n = 1), v) northwest (n = 5), vi) north-central large (n = 4), vii) southwest small (n = 11), and viii) southwest large (n = 2) (Figure 2b). We made a separate class for the six largest catchments in the north-central and southwestern regions (> 10 000 km²; the Ikopa, Betsiboka, Kamoro, Onilahy and Mangoky rivers) as each of these catchments encompasses multiple regions and nested catchments (Figure S2 and S3).

3.3 Statistical analyses

We performed a suite of statistical analyses on the dataset to identify the environmental variables that explain most spatial variations in ^{10}Be erosion rates. These were i) correlation and factor analysis, ii) stepwise multiple linear regression analysis, and iii) random (within-between) models. All results are reported at the 95% confidence level and were obtained using R v4.0.5.

Correlation and factor analysis

We calculated Spearman rank correlation coefficients to test for relationships between ^{10}Be erosion rates and different environmental variables. Rank coefficients are robust to outliers and are not linked to the distribution of the data. We also performed a factor analysis, which groups correlated variables into a smaller number of factors to extract a few common latent characteristics from a large set of variables. The factors are linear combinations of the original variables, and the factor loadings are the correlations between the original variables and the factors (Bartholomew et al., 2011; Kaiser, 1958; Starke et al., 2017). We calculated the factor scores using a varimax rotation and used the Kaiser criterion to determine the optimal number of factors (Kaiser, 1958). All factor analyses were performed using the nFactors package (Raiche, 2020).

Stepwise multiple linear regression

We performed stepwise multiple linear regressions to identify the variables that add significant explanatory power to the multivariate model. We used a forward and backward algorithm, where the regression model was built from the environmental variables by adding and removing predictors based on Akaike Information Criterion (AIC) (using the CRAN-olsrr package, Hebbali, 2020). We did this analysis on the full dataset and separately for the regions that contain sufficient observations (n > 10).

Random (within-between) models

Multilevel data structures occur when individuals or measurements (level 1) are nested within a geographical or social context (level 2, cross-sectional data). In such a framework, multilevel modelling by means of random effect (RE) and random within-between (REWB) models provides a means to identify the spatial scale at which most or least variation occurs, and to indicate the relative importance of different variables in explaining this variation (Bell et al., 2019; Jones, 1993). Our dataset can be considered as a cross-sectional multilevel data structure, where individual catchments i (level 1) are clustered into groups j (regions, level 2). Here, we give a short overview of the equations describing an REWB model; full details are provided in Text S1.3.

In a single level linear regression, the response variable y is predicted based on predictor variable x:

$$y_i = \beta_0 + \beta_1 x_i + (\epsilon_i) \tag{7}$$

β_0 and β_1 are fixed and unchanging parameters for the intercept and the slope and ϵ_i signifies the residual variance.

This equation only considers the variations observed at the level of the individuals i (level 1). To account for level-2 entries (different regions, j), it is required to allow the intercept μ_{oj} and slope μ_{1j} of the different regions to vary around the overall intercept β_0 and slope β_1, resulting in a random two-level model with varying intercept and slope:

$$y_{ij} = \beta_0 + \beta_1 x_{ij} + (\mu_{0j} + \mu_{1j} x_{ij} + \epsilon_{ij}) \tag{8}$$

The fixed part of the equation consists of the mean intercept and slope (β_0 and β_1) and the random part is given between by brackets with μ_{oj} the random intercept, μ_{1j} the random slope, and ϵ_{ij} the residual variance. The importance of the random part can be assessed from the variance of the slope and intercept.

While this random model allows varying slopes and intercepts for different regions, it does not yet allow to explicitly assess which variables explain differences between the different catchments (*within effect* at level 1) and between the different regions (*between effect* at level 2). Random within-between models allow to make this distinction explicit, by de- and group-meaning the predictors: the mean predictor value of each region is calculated and subtracted from the individual predictor values.

$$y_{ij} = \beta_0 + \beta_{1W}(x_{ij} - \bar{x_i}) + \beta_{2B}\bar{x_i} + (\mu_{0j} + \mu_{1j}(x_{ij} - \bar{x_i}) + \epsilon_{ij}) \tag{9}$$

$\bar{x_i}$ is the mean variable value for the region (group-mean) and indicates the between-effect, i.e. the difference between the different regions. $(x_{ij} - \bar{x_i})$ are the demeaned variable values per region indicating the within-effect, i.e. the difference between the different catchments. Only significant fixed and random effects were retained ($p < 0.05$) and we selected the model with the lowest AIC for each model type (Akaike, 1987).

4 Results

First, we investigated if there is a spatial pattern in ^{10}Be erosion rates in Madagascar. Next, we present the results of our statistical analyses to identify the environmental factors that explain most variation in ^{10}Be erosion rates. Finally, we assessed how ^{10}Be concentrations changed over time using river terrace samples

4.1 Spatial variations in ^{10}Be erosion rates

Three outliers with low ^{10}Be concentrations (and corresponding high ^{10}Be erosion rates) were identified and excluded from further analysis as they were associated with mass wasting processes or dam and bridge construction works near the sampling locations (id = 30, 32, 37, Table S1, Figure 3). ^{10}Be erosion rates range between 2.4 and 51.1 mm kyr^{-1}, with mean and median values for the full dataset of 16.6 and 12.7 mm kyr^{-1}, respectively (Table S1, Figure 2a)
The lowest ^{10}Be erosion rates are observed on the central highlands (7.5 ± 3.0 mm kyr^{-1}, n = 25), within the Alaotra-Ankay graben (11.0 ± 4.2 mm kyr^{-1}, n = 11), and for the large catchments in the north-central part (11.2 ± 0.9 mm kyr^{-1}, n = 3). Higher ^{10}Be erosion rates are found on the eastern escarpment (20.0 ± 10.1 mm kyr^{-1}, n = 3), in the northwest (31.0 ± 12.2 mm kyr^{-1}, n = 5), and in the small (29.0 ± 12.4 mm kyr^{-1}, n = 11) and large (22.0 ± 7.2 mm kyr^{-1}, n = 2) catchments of the southwest (Figure 2 and 3). While within-region variation in ^{10}Be erosion rates is limited for the central highlands, AAG and north-central large watersheds, considerable variation can be observed on the escarpment, with generally higher ^{10}Be erosion rates in the northern part of the escarpment compared to the southern part (Figure 2 and 3).

4.2 Factors explaining variations in erosion rates

4.2.1 Correlation and factor analysis

A total of 15 different environmental variables are examined to explain observed variations in ^{10}Be erosion rates. As a first step, we test for possible co-linearity by means of correlation and factor analysis for the full dataset.

Spearman rank correlation coefficients (ρ) indicate strong (and expected) positive correlations between the topographic variables of mean catchment gradient, relief, roughness, and normalized channel steepness k_{sn} (ρ between 0.58 and 0.99, Figure 4). These variables also positively correlate with precipitation (ρ of 0.42 to 0.65) and show a negative relationship with lithological erodibility (LE) and bioclimate (ρ -0.47 to -0.79, Figure 4). These variables (gradient, relief, roughness, k_{sn}, LE, precipitation and bioclimate) all have high absolute factor loadings on the first factor, which thus mainly covers differences in topography, bioclimate and lithology (Table 1). The three river concavity indices (SCI, θ, and θ_t) also strongly co-vary (ρ of 0.77 to 0.88), and are negatively correlated with the ^{10}Be erosion rates (ρ = -0.33 to -0.40, Figure 4) and constitute of the second identified factor (Table 1). The third factor has high factor loadings for seismic events, PGA and lavaka density (Table 1), for which positive correlations were observed, indicating that higher lavaka densities are found for catchments with higher seismic activity (Figure 4). Larger catchments are associated with higher relief and plot on the fourth factor axis (Figure 4, Table 1).

When considering the full dataset, ^{10}Be erosion rates are negatively correlated with stream concavity (Factor 2, Table 1, ρ between -0.33 and -0.40, Figure 4), but show the strongest negative correlation with mean catchment elevation (ρ = -0.54, Figure 4, Figure S6). Furthermore, a negative correlation with lavaka density (ρ = -0.31) and a small but significant positive correlation with LE (ρ = 0.25) is observed (Figure 4, Figure S6). When considering the full dataset (n = 88) this suggests that ^{10}Be erosion rates tend to increase where the lithology is weaker (higher LE), when stream profiles become less concave (move away from equilibrium) and when lavaka densities decrease (Figure 4, Figure S6). The latter correlation is counterintuitive as one would expect higher inferred erosion rates when there are more lavaka. In this case the effect of elevation may play a role: lavaka are only found on the higher central highlands where long-term erosion rates are lower (ρ = 0.34, Figure 1, 4, 3, and S6).

4.2.2 Stepwise Linear regression

Stepwise linear regressions were performed for both the full dataset and subsets of the different regions containing a sufficient number of sampled catchments. Similar to the outcomes of the correlation and factor analysis, elevation, stream concavity θ and lithological erodibility significantly contribute to explaining 43% of the observed variations in ^{10}Be erosion rates when considering the full dataset (n = 88) (Table 2, Figure S6).

Seismic events are the only included variable for the central highlands-region (n = 25) and explain 41% of the observed variation. Also for the Alaotra-Ankay graben (n = 11) and the small southwestern catchments (n = 11) only one variable is included in the stepwise linear model, being the lavaka density (R^2 = 0.23) and lithological erodibility (R^2 = 0.23), respectively. Most variation in ^{10}Be erosion rates on the eastern escarpment (n = 30) is associated with seismic events (R^2 = 0.39), where additional variation is explained by lithological erodibility, θ_t, elevation and precipitation, adding up to an R^2 of 0.55 (Table 2, Figure S6).

The relationships between ^{10}Be erosion rates and stream concavity, elevation and precipitation are negative for all the considered datasets, and positive when considering seismic events and lavaka densities (Table 2, Figure S6). When considering the graben region separately we obtain a positive relationship between lavaka densities and erosion rates (Table 2), strengthening the hypothesis that the negative correlation for the full dataset is related to another underlying factor like elevation (Figure 4). Both a positive (full dataset) and negative (eastern escarpment and SW small) relationship between ^{10}Be erosion rate and lithological erodibility is observed (Table 2, Figure S6), where a theoretical increase in ^{10}Be erosion rates with increasing erodibility would be expected. LE values for the catchments on the eastern escarpment are all equal and low except for two catchments, likely resulting in this spurious relationship (Figure S6). Similarly, the negative relationship for the southwestern catchments strongly hinges on one catchment with relatively high LE values and relatively low erosion rates, whereas all other erosion values vary widely for a rather narrow variation in LE (Figure S6).

4.2.3 Random (within-between) models

When applying a multiple linear regression (cfr. Equation 7) to our full dataset (n=88) we only consider fixed effects to explain variations in ^{10}Be erosion rates at catchment-level. In this case the significant negative variables that are included in the model are elevation and θ, with a positive coefficient for lithological erodibility ($R^2 = 0.38$, AIC = 642, residual variance = 56.13, Table 3, Table 2). In a model where the intercept is allowed to vary for the different regions (Random Intercept, Table 3), θ and seismicity are included as significant fixed effects. The model results in a conditional R^2 of 0.74. When also allowing random regression slopes for the different regions (cfr. Equation 8), elevation becomes the only significant fixed effect and seismic events and SCI are retained as significant random effects that have a varying regression slope and intercept for the different regions. This results in a slightly lower conditional R^2 of 0.62 when compared to the random intercept model (Table 3).
While these random models allow to identify the most important fixed effects and have a clearly higher explanatory power in comparison to a multiple linear regression model they do not allow us to clearly identify the environmental variables that explain variation between the different regions (between effect at level 2) and between the different catchments (within effect at level 1), which is explicitly included in the random within-between model (REWB cfr. Equation 9).
When applying a REWB model with random intercept to our dataset, the within effect of θ and seismicity are included in the fixed part of the model ($R^2 = 0.63$), indicating that these factors explain most differences between the individual catch-

ments: more convex and seismically active catchments have higher ^{10}Be erosion rates (Table 3). The REWB model where also random slopes are included shows that stream concavity, seismic events and lavaka density explain most of the variation in ^{10}Be erosion rates between the different regions, where the random regression slope of seismicity explains additional differences between the individual catchments of a region. This results in a R^2 of 0.73 for the full REWB model, and the lowest AIC of all models considered (Table 3).

In general, the RE(WB) models identify stream concavity (θ or SCI), seismicity, and lavaka density as the most important environmental variables that explain variations in ^{10}Be erosion rates both between and within regions for concavity and seismicity, while lavaka density is only associated with differences between regions. Specifically accounting for the multilevel structure of the data by including the different regions as a random effect has allowed to identify the main environmental variables that explain differences in ^{10}Be erosion rates, thereby omitting variables like elevation that explained most variation in a simple stepwise linear regression (R^2 = 0.27, Table 2) or correlation analysis (ρ = -0.46, Figure 4) but mainly reflected the differences in physical characteristics of the different regions instead of the actual driving factors.

The best performing model (REWB slope, Table 3) captures the observed variations in ^{10}Be erosion rates relatively well for the central highlands, Alaotra-Ankay Graben and eastern escarpment (Figure 5). The general trend in ^{10}Be erosion rates for the eastern escarpment is represented in the predicted values, but the range of the predicted values is smaller than the one of the observations (Figure 5). The remainder of the variation in ^{10}Be erosion rates on the escarpment is likely linked with the area of the catchment that is located on the plateau or in the plain, which is a variable that has not been considered in these analyses but is known to vary for the considered catchments (Wang et al., 2021). The model fails at predicting the observed variations in ^{10}Be erosion rates of the catchments in the southwest and northwest (Figure 5). The stepwise linear regression pointed out that variations in lithological erodibility were associated with variations in ^{10}Be erosion rates in the southwestern catchments, which is a factor that is not considered in the REWB slopes model, though this relationship is likely spurious as it strongly hinges on one observation (Table 2). We therefore conclude that the considered variables do not explain the significant variations in ^{10}Be erosion rates in the southwestern region. The small number of observations in the northwest (n = 5) likely explains the weak explanatory power of the model in this region, as the number of observations of each region is considered during model optimization (Jones, 1993; Bell et al., 2019).

4.3 Temporal variations in ^{10}Be erosion rates

Because ^{10}Be integrates over long timescales, it can be difficult to determine whether low calculated rates reflect a former state of the landscape, with recent increases in erosion rate as yet not detectable in the ^{10}Be system; or whether high measured rates reflect recent increases in erosion sufficient to swam the older signal versus the possibility that the long-term rates are high. One way to differentiate recent from background rates is to compare modern river ^{10}Be with measurements from older deposits of the same rivers. At four locations suitable terrace sampling locations containing datable material were found (Table S1). Modern river ^{10}Be concentrations are higher than terrace concentrations for the two largest catchments, suggesting lower recent erosion rates (Figure 6b). However, modern ^{10}Be concentrations are lower than terrace concentrations for the smallest catchments, suggesting higher current erosion rates. While differences are small, higher current ^{10}Be erosion rates were found for catchments with higher lavaka densities, which might explain the lower current ^{10}Be concentrations in river sediment (Figure 6b).

5 Discussion

The new ^{10}Be data confirm previously reported low ^{10}Be erosion rates for Madagascar, which range between 4 and 52.9 mm kyr^{-1} (Cox et al., 2009; Wang et al., 2021). These rates are amongst the lowest globally reported rates, and are well below the global mean and median values of 218 and 54 mm kyr^{-1} reported by Portenga and Bierman (2011), and the more recent median value of 76.7 mm kyr^{-1} of Codilean et al. (2018). We find clear spatial patterns, where the values are systematically higher for the catchments on the escarpment that drain to the east, compared to the backslope catchments that drain to the west, when accounting for differences in LE (Figure 3, Figure 2, Table S1).

Our analysis illustrates that a simple statistical analysis does not provide a full insight into the environmental factors controlling variations in long-term ^{10}Be erosion rates in the complex and diverse setting of Madagascar. When considering the full dataset, elevation is the most important environmental factor, where higher catchments were associated with lower ^{10}Be erosion rates (Table 2, Figure 4). However, a more sophisticated REWB analysis clearly shows that this association is spurious: the regions located at higher elevations do have geomorphological characteristics that differ from those at lower altitudes. REWB models do allow to identify the factors that control variations between and within regions. What is clear from our analysis is that a model that allows for regional stratification and wherein the coefficients associated with different explanatory values are allowed to vary by region, thereby accounting for both differences between and differences within regions, explains a much larger fraction of the variance observed in comparison to more classical models such as multiple regression analysis. When explicitly considering the different regions in the REWB model, the main environmental factors that strongly correlate with spatial variations in ^{10}Be erosion rates between the different regions are stream concavity, seismicity, and lavaka density, where differences in seismic events explain additional variation in ^{10}Be erosion rates within the regions (Table 3).

5.1 Driving forces of low long-term erosion rates

The central highland values (2.5 - 15.2 mm kyr^{-1}, Table S1, Figure 3) are comparable to those from upland plateaus elsewhere, for example 9.6 $\pm$ 0.8 mm kyr^{-1}

for the Western Ghats (Mandal et al., 2015), 2.6 - 6.2 mm kyr^{-1} in Sri Lanka (Vanacker et al., 2007b), 5.0 $\pm$ 0.5 mm kyr^{-1} in Southern Brazil (Schoonejans et al., 2017), and 10 mm kyr $^{-1}$ in southeast Australia (Godard et al., 2019). We infer that in the absence of active tectonics, physical long-term erosion rates in (sub)-tropical environments are low to very low, despite a strong relief and an erosive climate (von Blanckenburg, 2004; Codilean et al., 2021). The low ^{10}Be erosion rates from the eastern escarpment of 2.8 to 43.7 mm kyr^{-1} are similar to, although somewhat lower than, values reported for other passive margin escarpments in Sri Lanka (26 - 71 mm kyr^{-1}, Vanacker et al. (2007b); von Blanckenburg (2004)), the Western Ghats in India (15 - 53 mm kyr^{-1} Mandal et al. (2015); Wang and Willett (2021)), the southeastern Australian escarpment (20 - 60 mm kyr^{-1}, Godard et al. (2019)), the Serra do Mar escarpment in Southern Brazil (11 - 26 mm kyr^{-1}, Salgado et al. (2014)), and the Blue ridge escarpment in the Southern Appalachians (5.4 - 49 mm kyr^{-1},(Linari et al., 2017)). Our lowest values are observed in the southern part of the escarpment, which has more subdued topography than the northern and central parts (Figure 3).

The highest ^{10}Be erosion rates are observed at the escarpment (when controlling for differences in LE), which is characterized by major knickpoints, indicating active rejuvenation of the landscape. Above this knickzone in the central highlands, the topography is at or close to steady state, resulting in the observed lower erosion rates. The overall low ^{10}Be erosion rates of the highlands cannot be explained by a weathering-limited system: the regolith is very thick in many parts of Madagascar, providing plenty of material that can potentially be eroded. It therefore seems that in (sub)-tropical environments where uplift is small or an uplift pulse did not yet propagate up to the catchment, that natural vegetation and the presence of a strong laterite can protect an erodible saprolite on steep terrain sufficiently well from an erosive climate to reduce ^{10}Be erosion rates to a minimum over periods spanning more than 100 kyr. The presence of this thick regolith cover may, however, also be the consequence of the observed low long-term erosion rates.

The negative correlation between ^{10}Be erosion rates and river concavity (Figure 4, Figure S7, Table 2, Table 3) indicates that the transient rivers of the eastern escarpment are characterized by higher erosion rates (Vanacker et al., 2015). This is in agreement with the inferred horizontal retreat of the eastern escarpment, which occurs at rates between 182 and 1886 mm kyr^{-1} (Wang et al., 2021; Wang and Willett, 2021). This observation is consistent with a model of steady retreat from the coastline since the time of rifting (Wang et al., 2021), similar to what has been suggested for the Western Ghats (Wang and Willett, 2021) and Sri Lanka (Vanacker et al., 2007b).

A similar link between river concavity and erosion rates was observed along an east-west transect through the tropical Andes by Vanacker et al. (2015). They furthermore found a clear positive relationship between ^{10}Be erosion rates and mean hillslope gradient and k_{sn} in the transient regions, which was absent for the catchments located upstream of the knickpoint in the inter-Andean basin. These rather low uniform erosion rates that seemed independent from local relief were explained by the more or less steady state of these catchments which have not yet experienced the pulse of relief rejuvenation that propagates through the escarpment (Vanacker et al., 2015).

While river concavity was clearly related to ^{10}Be erosion rates in our dataset, we did not see a relationship with overall slope gradient or river steepness, even in the steep catchments of the eastern escarpment (Figure 4 and Figure S6). A positive relationship between river and slope steepness and ^{10}Be erosion rates has, however, been observed in a variety of active and passive tectonic settings (e.g. Riebe et al., 2000; Abbühl et al., 2011; Schaller et al., 2001; Campforts et al., 2020; Codilean et al., 2021; Matmon et al., 2003; Linari et al., 2017). The absence of a clear pattern for our upland catchments (central highland and Alaotra-Ankay graben) might be similar to the inter-Andean setting: the pulse of relief rejuvenation that propagates through the escarpment has not yet arrived, leaving these catchments in dynamic steady-state (Vanacker et al., 2015; Kwang et al., 2021; Beeson et al., 2017). The absence of a clear relationship on the escarpment might be related to the regular occurrence of river captures, where gentle highland rivers that previously drained to the west now drain to the east, thereby affecting the calculated average values (Wang et al., 2021). Wang et al. (2021) furthermore also reported low confidence in the channel steepness calculations given the transience of the river profiles and the large intra-basin variance, which will also apply to our analysis.

Seismicity in steep terrain can cause mass wasting and can lower the rock strength as it may enhance rock fracturing, resulting in higher chemical weathering and a lowering of the strength over greater depth (Riebe et al., 2000; von Blanckenburg, 2004, 2005). This may explain the observed positive correlation between ^{10}Be erosion rates and seismic activity, which is especially marked in the northern part of the eastern escarpment, parts of the central highlands and in the Alaotra-Ankay graben (Table 2, Figure S6 and Table 3). The seismic activity and associated higher ^{10}Be erosion rates can also be linked with the rifting of the Alaotra-Ankay graben. This results in local base level changes and tectonically induced faults and joints that rejuvenate the topography, starting a new phase of adjustment of the topography by changing erosion rates (Mietton et al., 2018; Kusky et al., 2010).

Measured ^{10}Be erosion rates of the catchments in the northwestern and southwestern basins are as high as the ones on the escarpment, despite the fact that they are low lying and have gentle relief (Figure S6, Table S4). The main difference with the other studied regions is that these catchments are underlain by more recent sedimentary deposits that have a higher lithological erodibility compared to the Precambrian basement, which may explain the relatively high rates observed in this area (Figure 4, Table 2, Figure S6).

5.2 The importance of deep chemical weathering

Recent studies have indicated the importance of deep chemical weathering in tropical regolith-covered landscapes like the highlands of Madagascar. Rates of landscape lowering inferred from cosmogenic nuclides apply to the material that is lost by both physical erosion and chemical weathering processes from the upper one to two meters, i.e. the penetration depth of cosmic rays. As the thick regolith shields deeper layers (> 2 m) from cosmogenic nuclide buildup, material that gets lost by chemical weathering processes below this depth will not be reflected in denudation rates inferred from cosmogenic nuclides. This can result in an underestimation of more than 100% of the actual landscape denudation rates (Riebe and Granger, 2013; Dixon et al., 2009; Ott et al., 2022). Chemical weathering rates inferred from dissolved river loads in Sri Lanka (which has a similar tectonic setting to Madagascar) were low (2 - 7 mm kyr^{-1}), but comparable to ^{10}Be erosion rates, indicating that ^{10}Be was capturing only about half of the actual denudation rate (2 - 11 mm kyr^{-1}) (von Blanckenburg, 2004). Similarly, Regard et al. (2016) estimated that deep chemical weathering accounts for 60% of the total denudation in a thick, highly weathered, regolith on the Cameroon craton. A recent study from Cuba furthermore indicated significant landscape-scale mass loss that was not reflected in *in-situ* ^{10}Be cosmogenic nuclide measurements (4 - 180 t km^{-2} yr^{-1} corresponding to 2 - 69 mm kyr^{-1} when ρ = 2.6 t m^3), with rock dissolution rates (24 - 154 t km^{-2} yr^{-1} corresponding to 9 - 59 mm kyr^{-1} when ρ = 2.6 t m^3) exceeding the latter in 15 of 22 basins (Campbell et al., 2022).

We made a first back-of-the-envelope calculation based on dissolved loads (Mg, Na, Si, K, Ca) and river discharge measurements during one hydrological year (July 2018 - September 2019) for the Ranofotsy river, a relatively small (406 km^2) catchment in the Lake Alaotra region (Figure 1c). We calculate a chemical weathering flux of 113 (50 - 194) t km^{-2} yr^{-1} for that year, suggesting chemical denudation rates of 42 (19 - 72) mm kyr^{-1} when assuming that weathering is not iso-volumetric (Text S1.4). These values for the central highlands of Madagascar are in the range of the estimates obtained by Campbell et al. (2022), but higher than the rates obtained for Sri Lanka. Even though this estimate entails large uncertainties, it suggests that mass loss through chemical weathering is probably a major (and hitherto unacknowledged) factor for regional denudation in Madagascar. Thus, the low ^{10}Be erosion rates in the central highlands, which do not exceed 20 mm kyr^{-1} (Figure 2, Table S1), may be measuring only a portion of the total denudation. Chemical weathering indices calculated from the elemental chemistry of the river bedload material draining the central highlands and eastern escarpment show that the erosion pattern is reflected in the weathering indices: weathering degrees are highest at the central plateau and on the eastern plain where erosion rates are low, and are lowest at the eastern escarpment which is characterized by high erosion rates (Wang, 2021). While these data confirm that weathering degrees are high, a systematic and long-term monitoring effort of solute fluxes in multiple catchments in the different regions is required to address this knowledge gap.

5.3 Impact of gully processes on long-term ^{10}Be and current erosion rates

The central highland and Alaotra-Ankay graben region are characterized by locally high lavaka densities, with lavaka that are on average 15 m deep (Cox et al., 2009; Voarintsoa et al., 2012). Lavaka incision and erosion appear to significantly impact ^{10}Be systematics (Table 2, Table 3, Figure 6a); a similar negative correlation between lavaka densities and ^{10}Be concentrations in the central highlands was also found by Cox et al. (2009). Lavaka density explains variations in ^{10}Be erosion rates between regions, but not within regions (Table 3). This seems to suggest that it is the general propensity of the region to the formation of lavaka which is associated with somewhat higher ^{10}Be erosion rates rather than current and past sediment production by lavaka.

^{10}Be concentrations from the floors of actively eroding lavaka were found to be as low as 0.8×10^5 atoms g^{-1}, only a tenth of topsoil concentrations, driving the inference that lavaka contribute 84% of sediment input to the fluvial system (Cox et al., 2009). Thus the deep saprolites with their low ^{10}Be concentrations significantly impact the average ^{10}Be concentration of the river sediments, thereby increasing the derived ^{10}Be erosion rates. In this regard lavaka behave similarly to mass wasting processes like landsliding (Quock et al., 2022; Grande et al., 2021; Yanites et al., 2009). Therefore caution is required when interpreting catchment-wide cosmogenic erosion rates in such terrain (von Blanckenburg, 2005).

While reliable regional estimates of current erosion and sediment export rates are not available for most regions in Madagascar, there are indications that current sediment export rates rates exceed long-term erosion rates by one or two orders of magnitude in some places. For the Ikopa catchment in the central highlands near Antananarivo a current erosion rate of 200 mm kyr^{-1} was derived from suspended sediment loads (360 t km^{-2} yr^{-1} assuming a bulk density (ρ) of 1.8 t m^{-3}, Mietton et al., 2020). Similar measurements for the Bevava and Sahamaloto reservoirs in the lake Alaotra region indicate current erosion rates of around 1 000 mm kyr^{-1} (Mietton et al., 2020, 2006). These higher rates in the lake Alaotra region were linked to high lavaka densities (Mietton et al., 2020, 2006). Brosens et al. (2022b) estimated that over the period 1949-2010s lavaka erode between 500 and 9 200 mm kyr^{-1} based on detailed measurements of changes in lavaka areas and related volumes in six small study areas in the region (7 - 129 t ha^{-1} yr^{-1}). Brosens et al. (2022a) and Broothaerts et al. (2022) furthermore showed that lavaka erosion and floodplain sedimentation rates have increased over the last millennium, and especially over the last few hundred years, and that these sediments are currently stored in the alluvial plains of the river network upstream of lake Alaotra. This might explain why ^{10}Be-inferred erosion rates in large catchments have not increased recently when compared to older river terrace concentrations, whereas those of smaller catchments have (Figure 6): sediments mobilized by a recent increase in lavaka erosion have not yet reached the outlet of larger catchments. This is to be expected, as several studies have shown that sediment residence times in alluvial environments are often thousands of years (Wittmann and von Blanckenburg, 2009; Hoffmann, 2015; Pizzuto et al., 2014).

6 Conclusion

A dataset of 99 detrital *in-situ* ^{10}Be concentrations covering major parts of Madagascar allowed us to assess how long-term denudation rates (excluding chemical weathering below the cosmic ray attenuation depth) vary over the island. Clear differences exist. Low ^{10}Be erosion rates of 7.5 $\pm$ 3.0 and 11.0 $\pm$ 4.2 mm kyr^{-1} were found in the central highlands and in the Alaotra-Ankay graben. This confirms that subtropical environments, even when characterized by strong relief and steep slopes, can be geomorphologically stable over long time spans. Higher and more variable rates were observed along the eastern escarpment (20.0 $\pm$ 10.1 mm kyr^{-1}), in the northwest (31.0 $\pm$ 12.2 mm kyr^{-1}), and the southwest (29.0 $\pm$ 12.4 mm kyr^{-1}). Higher ^{10}Be erosion rates were associated with lower river concavity (more convex shaped rivers) and higher seismic activity both at the level of individual catchments as well as at the regional level, while higher lavaka densities explain regional variations. No relationship between ^{10}Be erosion rates and slope gradient or river steepness was observed, which brings into question the general applicability of fluvial metrics to constrain vertical incision rates in a slowly eroding landscape such as Madagascar. While ^{10}Be concentrations suggest that rates of landscape change in Madagascar are low, there are indications that chemical weathering rates may outpace CRN-derived denudation rates, pointing to the importance of deep weathering and removal of dissolved materials. In thick regolith-mantled landscapes, mass losses by deep weathering and subsurface dissolution should be considered alongside with mass losses by physical erosion.

References

Aalto, R., Dunne, T., and Guyot, J. L.: Geomorphic Controls on Andean Denudation Rates, The Journal of Geology, 114, 85–99, https://doi.org/10.1086/498101, 2006.

Abbühl, L. M., Norton, K. P., Jansen, J. D., Schlunegger, F., Aldahan, A., and Possnert, G.: Erosion rates and mechanisms of knickzone retreat inferred from 10Be measured across strong climate gradients on the northern and central Andes Western Escarpment, Earth Surface Processes and Landforms, 36, 1464–1473, https://doi.org/10.1002/esp.2164, 2011.

Akaike, H.: Factor analysis and AIC, Psychometrika, 52, 317–332, https://doi.org/10.1007/BF02294359, 1987.

Bartholomew, D., Knott, M., and Moustaki, I.: Latent variable models and factor analysis. A unified approach, John Wiley & Sons Ltd, Chichester, UK, 3rd edn., 2011.

Bartley, R., Croke, J., Bainbridge, Z. T., Austin, J. M., and Kuhnert, P. M.: Combining contemporary and long-term erosion rates to target erosion hot-spots in the Great Barrier Reef, Australia, Anthropocene, 10, 1–12, https://doi.org/10.1016/j.ancene.2015.08.002, 2015.

Battistini, R.: Madagascar relief and main types of landscape, in: Biogeography and ecology in Madagascar, edited by Battistini, R. and Richard-Vindard, G., p. 765, Springer, Dordrecht, 1972.

Beeson, H. W., McCoy, S. W., and Keen-Zebert, A.: Geometric disequilibrium of river basins produces long-lived transient landscapes, Earth and Planetary Science Letters, 475, 34–43, https://doi.org/10.1016/j.epsl.2017.07.010, 2017.

Bell, A., Fairbrother, M., and Jones, K.: Fixed and random effects models: making an informed choice, Quality and Quantity, 53, 1051–1074, https://doi.org/10.1007/s11135-018-0802-x, 2019.

Bierman, P. and Steig, E. J.: Estimating rates of denudation using cosmogenic isotope abundance in sediment, Earth Surface Processes and Landforms, 21, 125–139, https://doi.org/10.1002/(SICI)1096-9837(199602)21:2<125::AID-ESP511>3.0.CO;2-8, 1996.

Broothaerts, N., Razanamahandry, V. F., Brosens, L., Campforts, B., Jacobs, L., Razafimbelo, T., Rafolisy, T., Verstraeten, G., Bouillon, S., and Govers, G.: Vegetation changes and sediment dynamics in the Lake Alaotra region, central Madagascar, The Holocene, p. 095968362211453, https://doi.org/10.1177/09596836221145376, 2022.

Brosens, L., Broothaerts, N., Campforts, B., Jacobs, L., Razanamahandry, V. F., Van Moerbeke, Q., Bouillon, S., Razafimbelo, T., Rafolisy, T., and Govers, G.: Under pressure: Rapid lavaka erosion and floodplain sedimentation in central Madagascar, Science of The Total Environment, 806, 150 483, https://doi.org/10.1016/j.scitotenv.2021.150483, 2022a.

Brosens, L., Campforts, B., Govers, G., Aldana-Jague, E., Razanamahandry, V. F., Razafimbelo, T., Rafolisy, T., and Jacobs, L.: Comparative analysis of the Copernicus, TanDEM-X, and UAV-SfM digital elevation models to estimate lavaka (gully) volumes and mobilization rates in the Lake Alaotra region (Madagascar), Earth Surface Dynamics, 10, 209–227, https://doi.org/10.5194/esurf-10-209-2022, 2022b.

Buchhorn, M., Smets, B., Bertels, L., De Roo, B., Lesiv, M., Tsendbazar, N., Linlin, L., and Tarko, A.: Copernicus Global Land Service: Land Cover 100m: Version 3 Globe 2015-2019: Product User Manual, Tech. rep., Zenodo, Geneve, https://doi.org/10.5281/zenodo.3938963, 2020.

Burgess, N., D'Amico Hales, J., Underwood, E., Dinerstein, E., Olson, D., Itoua, I., Schipper, J., Ricketts, T., and Newman, K.: Terrestrial eco-regions of Africa and Madagascar: A conservation assessment., September 2016, Island Press, Washington, DC, 2004.

Campbell, M. K., Bierman, P. R., Schmidt, A. H., Sibello Hernández, R., García-Moya, A., Corbett, L. B., Hidy, A. J., Cartas Águila, H., Guillén Arruebarrena, A., Balco, G., Dethier, D., and Caffee, M.: Cosmogenic nuclide and solute flux data from central Cuban rivers emphasize the importance of both physical and chemical mass loss from tropical landscapes, Geochronology, 4, 435–453, https://doi.org/10.5194/gchron-4-435-2022, 2022.

Campforts, B., Vanacker, V., Herman, F., Vanmaercke, M., Schwanghart, W., Tenorio, G. E., Willems, P., and Govers, G.: Parameterization of river incision models requires accounting for environmental heterogeneity: Insights from the tropical Andes, Earth Surface Dynamics, 8, 447–470, https://doi.org/10.5194/esurf-8-447-2020, 2020.

Codilean, A., Fülöp, R.-H., Munack, H., Wilcken, K., Cohen, T., Rood, D., Fink, D., Bartley, R., Croke, J., and Fifield, L.: Controls on denudation along the East Australian continental margin, Earth-Science Reviews, 214, 103 543, https://doi.org/10.1016/j.earscirev.2021.103543, 2021.

Codilean, A. T., Munack, H., Cohen, T. J., Saktura, W. M., Gray, A., and Mudd, S. M.: OCTOPUS: An open cosmogenic isotope and luminescence database, Earth System Science Data, 10, 2123–2139, https://doi.org/10.5194/essd-10-2123-2018, 2018.

Collins, A. S. and Windley, B. F.: The Tectonic Evolution of Central and Northern Madagascar and Its Place in the Final Assembly of Gondwana, The Journal of Geology, 110, 325–339, https://doi.org/10.1086/339535, 2002.

Corbett, L. B., Bierman, P. R., and Rood, D. H.: An approach for optimizing in situ cosmogenic 10Be sample preparation, Quaternary Geochronology, 33, 24–34, https://doi.org/10.1016/j.quageo.2016.02.001, 2016.

Cornet, A.: Essai de cartographie bioclimatique à Madagascar, Tech. rep., ORSTROM, Paris, URL https://www.documentation.ird.fr/hor/fdi:06946, 1974.

Cox, R., Bierman, P., Jungers, M. C., and Rakotondrazafy, A. F. M.: Erosion Rates and Sediment Sources in Madagascar Inferred from 10Be Analysis of Lavaka, Slope, and River Sediment, The Journal of Geology, 117, 363–376, https://doi.org/10.1086/598945, 2009.

Cox, R., Zentner, D. B., Rakotondrazafy, A. F. M., and Rasoazanamparany, C. F.: Shakedown in Madagascar: Occurrence of lavakas (erosional gullies) associated with seismic activity, Geology, 38, 179–182, https://doi.org/10.1130/G30670.1, 2010.

Crowley, B. E.: A refined chronology of prehistoric Madagascar and the demise of the megafauna, Quaternary Science Reviews, 29, 2591–2603, https://doi.org/10.1016/j.quascirev.2010.06.030, 2010.

de Wit, M. J.: Madagascar: Heads It's a Continent, Tails It's an Island, Annual Review of Earth and Planetary Sciences, 31, 213–248, https://doi.org/10.1146/annurev.earth.31.100901.141337, 2003.

Demoulin, A.: Testing the tectonic significance of some parameters of longitudinal river profiles: the case of the Ardenne (Belgium, NW Europe), Geomorphology, 24, 189–208, https://doi.org/10.1016/S0169-555X(98)00016-6, 1998.

Dixon, J. L., Heimsath, A. M., and Amundson, R.: The critical role of climate and saprolite weathering in landscape evolution, Earth Surface Processes and Landforms, 34, 1507–1521, https://doi.org/10.1002/esp.1836, 2009.

Donque, G.: The climatology of Madagascar, in: Biogeography and ecology in Madagascar, edited by Battistini, R. and Richard-Vindard, G., p. 765, Springer, Dordrecht, 1972.

Douglass, K., Hixon, S., Wright, H. T., Godfrey, L. R., Crowley, B. E., Manjakahery, B., Rasolondrainy, T., Crossland, Z., and Radimilahy, C.: A critical review of radiocarbon dates clarifies the human settlement of Madagascar, Quaternary Science Reviews, 221, 105 878, https://doi.org/10.1016/j.quascirev.2019.105878, 2019.

Dunai, T. J.: Cosmogenic Nuclides. Principles, Concepts and Applications in the Earth Surface Sciences, Cambridge University press, New York, 2010.

Eagles, G. and Hoang, H. H.: Cretaceous to present kinematics of the Indian, African and Seychelles plates, Geophysical Journal International, 196, 1–14, https://doi.org/10.1093/gji/ggt372, 2014.

Farr, T. G., Rosen, P. A., Caro, E., Crippen, R., Duren, R., Hensley, S., Kobrick, M., Paller, M., Rodriguez, E., Roth, L., Seal, D., Shaffer, S., Shimada, J., Umland, J., Werner, M., Oskin, M., Burbank, D., and Alsdorf, D. E.: The shuttle radar topography mission, Reviews of Geophysics, 45, https://doi.org/10.1029/2005RG000183, 2007.

Flint, J. J.: Stream gradient as a function of order, magnitude, and discharge, Water Resources Research, 10, 969–973, https://doi.org/10.1029/WR010i005p00969, 1974.

Funk, C. C., Peterson, P. J., Landsfeld, M. F., Pedreros, D. H., Verdin, J. P., Rowland, J. D., Romero, B. E., Husak, G. J., Michaelsen, J. C., and Verdin, A. P.: A Quasi-Global Precipitation Time Series for Drought Monitoring, Tech. rep., USGS, 2014.

Garcin, Y., Vincens, A., Williamson, D., Guiot, J., and Buchet, G.: Wet phases in tropical southern Africa during the last glacial period, Geophysical Research Letters, 33, 1–4, https://doi.org/10.1029/2005GL025531, 2006.

Gasse, F. and Van Campo, E.: Late Quaternary environmental changes from a pollen and diatom record in the southern tropics (Lake Tritrivakely, Madagascar), Quaternary Research, 167, 287–308, https://doi.org/10.1006/qres.1998.1967, 2001.

Gibbons, A. D., Whittaker, J. M., and Müller, R. D.: The breakup of East Gondwana: Assimilating constraints from Cretaceous ocean basins around India into a best-fit tectonic model, Journal of Geophysical Research: Solid Earth, 118, 808–822, https://doi.org/10.1002/jgrb.50079, 2013.

Godard, V., Dosseto, A., Fleury, J., Bellier, O., and Siame, L.: Transient landscape dynamics across the Southeastern Australian Escarpment, Earth and Planetary Science Letters, 506, 397–406, https://doi.org/10.1016/j.epsl.2018.11.017, 2019.

Grande, A., Schmidt, A. H., Bierman, P. R., Corbett, L. B., López-Lloreda, C., Willenbring, J., McDowell, W. H., and Caffee, M. W.: Landslides, hurricanes, and sediment sourcing impact basin-scale erosion estimates in Luquillo, Puerto Rico, Earth and Planetary Science Letters, 562, 116 821, https://doi.org/10.1016/j.epsl.2021.116821, 2021.

Granger, D. E., Kirchner, J. W., and Finkel, R.: Spatially averaged long-term erosion rates measured from in-situ produced cosmogenic nuclides in alluvial sediment, Journal of Geology, 104, 249–257, 1996.

Hansford, J., Wright, P. C., Rasoamiaramanana, A., Pérez, V. R., Godfrey, L. R., Errickson, D., Thompson, T., and Turvey, S. T.: Early Holocene human presence in Madagascar evidenced by exploitation of avian megafauna, Science Advances, 4, 1–7, https://doi.org/DOI: 10.1126/sciadv.aat6925, 2018.

Hebbali, A.: olsrr: Tools for building OLS regression models, URL https://cran.r-project.org/package=olsrr, 2020.

Hewawasam, T., von Blanckenburg, F., Schaller, M., and Kubik, P.: Increase of human over natural erosion rates in tropical highlands constrained by cosmogenic nuclides, Geology, 31, 597–600, https://doi.org/10.1130/0091-7613(2003)031<0597:IOHONE>2.0.CO;2, 2003.

Hoffmann, T.: Sediment residence time and connectivity in non-equilibrium and transient geomorphic systems, https://doi.org/10.1016/j.earscirev.2015.07.008, 2015.

Howard, A. D.: A detachment-limited model of drainage basin evolution, Water Resources Research, 30, 2261–2285, https://doi.org/10.1029/94WR00757, 1994.

Institut et Observatoire de Géophysique D'Antananarivo: Liste de seismes locaux enregistres par le reseau sismique Malgache en 1996, Tech. rep., Ministère de l'Enseignement supérieur, Madagascar. Institut et Observatoire de Géophysique D'Antananarivo, 2008.

Jones, K.: Using multilevel models for survey analysis, Journal of the Market Research Society, 35, 249–265, 1993.

Joseph, G. S. and Seymour, C. L.: Madagascan highlands: Originally woodland and forest containing endemic grasses, not grazing-adapted grassland: Madagascar's vanished woodland, Proceedings of the Royal Society B: Biological Sciences, 287, 1–7, https://doi.org/10.1098/rspb.2020.1956rspb20201956, 2020.

Joseph, G. S., Rakotoarivelo, A. R., and Seymour, C. L.: How expansive were Malagasy Central Highland forests, ericoids, woodlands and grasslands? A multidisciplinary approach to a conservation conundrum, Biological Conservation, 261, 109 282, https://doi.org/10.1016/j.biocon.2021.109282, 2021.

Kaiser, H. F.: The varimax criterion for analytic rotation in factor analysis, Psychometrika, 23, 187–200, https://doi.org/10.1007/BF02289233, 1958.

Kober, F., Zeilinger, G., Hippe, K., Marc, O., Lendzioch, T., Grischott, R., Christl, M., Kubik, P., and Zola, R.: Tectonic and lithological controls on denudation rates in the central Bolivian Andes, Tectonophysics, 657, 230–244, https://doi.org/10.1016/j.tecto.2015.06.037, 2015.

Koechlin, J., Guillaumet, J.-L., and Morat, P.: Biogeography and Ecology in Madagascar, vol. 21 of *Monographiae Biologicae*, Springer Netherlands, Dordrecht, https://doi.org/10.1007/978-94-015-7159-3, 1972.

Kohl, C. and Nishiizumi, K.: Chemical isolation of quartz for measurement of in-situ -produced cosmogenic nuclides, Geochimica et Cosmochimica Acta, 56, 3583–3587, https://doi.org/10.1016/0016-7037(92)90401-4, 1992.

Kukla, G.: Saalian supercycle, Mindel/Riss interglacial and Milankovitch's dating, Quaternary Science Reviews, 24, 1573–1583, https://doi.org/10.1016/j.quascirev.2004.08.023, 2005.

Kusky, T. M., Toraman, E., Raharimahefa, T., and Rasoazanamparany, C.: Active tectonics of the Alaotra–Ankay Graben System, Madagascar: Possible extension of Somalian–African diffusive plate boundary?, Gondwana Research, 18, 274–294, https://doi.org/10.1016/j.gr.2010.02.003, 2010.

Kutzbach, J. E., Guan, J., He, F., Cohen, A. S., Orland, I. J., and Chen, G.: African climate response to orbital and glacial forcing in 140,000-y simulation with implications for early modern human environments, Proceedings of the National Academy of Sciences of the United States of America, 117, 2255–2264, https://doi.org/10.1073/pnas.1917673117, 2020.

Kwang, J. S., Langston, A. L., and Parker, G.: The role of lateral erosion in the evolution of nondendritic drainage networks to dendricity and the persistence of dynamic networks, Proceedings of the National Academy of Sciences of the United States of America, 118, 1–6, https://doi.org/10.1073/pnas.2015770118, 2021.

Lague, D.: The stream power river incision model: Evidence, theory and beyond, Earth Surface Processes and Landforms, 39, 38–61, https://doi.org/10.1002/esp.3462, 2014.

Linari, C. L., Bierman, P. R., Portenga, E. W., Pavich, M. J., Finkel, R. C., and Freeman, S. P.: Rates of erosion and landscape change along the Blue Ridge escarpment, southern Appalachian Mountains, estimated from in situ cosmogenic 10Be, Earth Surface Processes and Landforms, 42, 928–940, https://doi.org/10.1002/esp.4051, 2017.

Mandal, S. K., Lupker, M., Burg, J.-P., Valla, P. G., Haghipour, N., and Christl, M.: Spatial variability of 10 Be-derived erosion rates across the southern Peninsular Indian escarpment: A key to landscape evolution across passive margins, Earth and Planetary Science Letters, 425, 154–167, https://doi.org/10.1016/j.epsl.2015.05.050, 2015.

Matmon, A., Bierman, P., Larsen, J., Southworth, S., Pavich, M., and Caffee, M.: Temporally and spatially uniform rates of erosion in the southern Appalachian Great Smoky Mountains, Geology, 31, 155–158, https://doi.org/10.1130/0091-7613(2003)031<0155:TASURO>2.0.CO;2, 2003.

McConnell, W. J. and Kull, C. A.: Deforestation in Madagacar. Debates over the island's forest cover and challenges of measuring forest changes, in: Conservation and Environmental Managament in Madagascar, edited by Scales, I. R., chap. 4, Taylor & Francis Group, 2014.

Mietton, M., Leprun, J.-C., Andrianaivoarivony, R., Dubar, M., Beiner, M., Erismann, J., Bonnier, F., Grisorio, E., Rafanomezana, J.-P., and Grandjean, P.: Ancienneté et vitesse d'érosion des lavaka à Madagascar, in: Érosion et gestion conservatoire de l'eau et de la fertilité des sols. Actes des journées scientifiques du réseau érosion et GCES de l'AUF, pp. 87–94, 2006.

Mietton, M., Gunnell, Y., Nicoud, G., Ferry, L., Razafimahefa, R., and Grandjean, P.: 'Lake' Alaotra, Madagascar: A late Quaternary wetland regulated by the tectonic regime, Catena, 165, 22–41, https://doi.org/10.1016/j.catena.2018.01.021, 2018.

Mietton, M., Gunnell, Y., Andriamitia, J., Crouzet, C., Montade, V., Jouannic, G., Nicoud, G., and Razafimahefa, R.: Neotectonics and pastoralism: How they impact flood regimes in Madagascar's highlands, Science of the Total Environment, 742, 140 633, https://doi.org/10.1016/j.scitotenv.2020.140633, 2020.

Mudd, S. M., Harel, M. A., Hurst, M. D., Grieve, S. W., and Marrero, S. M.: The CAIRN method: Automated, reproducible calculation of catchment-averaged denudation rates from cosmogenic nuclide concentrations, Earth Surface Dynamics, 4, 655–674, https://doi.org/10.5194/esurf-4-655-2016, 2016.

Nassor, A. and Jury, M. R.: Intra-seasonal climate variability of Madagascar. Part 1: Mean summer conditions, Meteorology and Atmospheric Physics, 65, 31–41, https://doi.org/10.1007/BF01030267, 1998.

Ott, R. F., Gallen, S. F., and Granger, D. E.: Cosmogenic nuclide weathering biases: corrections and potential for denudation and weathering rate measurements, Geochronology, 4, 455–470, https://doi.org/10.5194/gchron-4-455-2022, 2022.

Pizzuto, J., Schenk, E. R., Hupp, C. R., Gellis, A., Noe, G., Williamson, E., Karwan, D. L., O'Neal, M., Marquard, J., Aalto, R., and Newbold, D.: Characteristic length scales and time-averaged transport velocities of suspended sediment in the mid-Atlantic Region, USA, Water Resources Research, 50, 790–805, https://doi.org/10.1002/2013WR014485, 2014.

Poggi, V., Durrheim, R., Tuluka, G. M., Weatherill, G., Gee, R., Pagani, M., Nyblade, A., and Delvaux, D.: Assessing seismic hazard of the East African Rift: a pilot study from GEM and AfricaArray, Bulletin of Earthquake Engineering, 15, 4499–4529, https://doi.org/10.1007/s10518-017-0152-4, 2017.

Portenga, E. W. and Bierman, P. R.: Understanding earth's eroding surface with 10Be, GSA Today, 21, 4–10, https://doi.org/10.1130/G111A.1, 2011.

Portenga, E. W., Bierman, P. R., Duncan, C., Corbett, L. B., Kehrwald, N. M., and Rood, D. H.: Erosion rates of the Bhutanese Himalaya determined using in situ-produced 10Be, Geomorphology, 233, 112–126, https://doi.org/10.1016/j.geomorph.2014.09.027, 2015.

Quock, M., Schmidt, A. H., Corbett, L. B., Bierman, P. R., Hidy, A. J., and Caffee, M.: Hurricanes alter 10 Be concentrations in tropical river sediment but do not change regional erosion rate estimates, Earth Surface Processes and Landforms, 1, 1–16, https://doi.org/10.1002/esp.5310, 2022.

Raiche, G.: nFactors: Parallel analysis and other non graphical solutions to the Cattell Scree test., URL `https://cran.r-project.org/package=nFactors`, 2020.

Rakotondraibe, T., Nyblade, A. A., Wysession, M. E., Durrheim, R. J., Rambolamanana, G., Aleqabi, G. I., Shore, P. J., Pratt, M. J., Andriampenomanana, F., Rümpker, G., and Rindraharisaona, E.: Seismicity and seismotectonics of Madagascar revealed by the 2011–2013 deployment of the island-wide MACOMO broadband seismic array, Tectonophysics, 790, 228 547, https://doi.org/10.1016/j.tecto.2020.228547, 2020.

Ramanantsoa, A. H.: Seismic observation in Madagascar, Bulletin of the International Institute of Seismology and Earthquake Engineering, 34, 59–69, 2000.

Reeves, C., Sahu, B., and de Wit, M.: A re-examination of the paleo-position of Africa's eastern neighbours in Gondwana, Journal of African Earth Sciences, 34, 101–108, https://doi.org/10.1016/S0899-5362(02)00011-8, 2002.

Regard, V., Carretier, S., Boeglin, J.-l., Ndam Ngoupayou, J.-R., Dzana, J.-g., Bedimo Bedimo, J.-P., Riotte, J., and Braun, J.-J.: Denudation rates on cratonic landscapes: comparison between suspended and dissolved fluxes, and 10Be analysis in the Nyong and Sanaga River basins, south Cameroon, Earth Surface Processes and Landforms, 41, 1671–1683, https://doi.org/10.1002/esp.3939, 2016.

Reimer, P. J., Baillie, M. G. L., Bard, E., Bayliss, A., Beck, J. W., Bertrand, C. J. H., Blackwell, P. G., Buck, C. E., Burr, G. S., Cutler, K. B., Damon, P. E., Edwards, R. L., Fairbanks, R. G., Friedrich, M., Guilderson, T. P., Hogg, A. G., Hughen, K. A., and Kromer, B.: INTCAL04 Terrestrial radiocarbon age calibration, 0-26 kyr BP, Radiocarbon, 46, 1029–1058, 2004.

Reinhardt, A. L., Kasper, T., Lochner, M., Bliedtner, M., Krahn, K. J., Haberzettl, T., Shumilovskikh, L., Rahobisoa, J. J., Zech, R., Favier, C., Behling, H., Bremond, L., Daut, G., and Montade, V.: Rain Forest Fragmentation and Environmental Dynamics on Nosy Be Island (NW Madagascar) at 1300 cal BP Is Attributable to Intensified Human Impact, Frontiers in Ecology and Evolution, 9, 783 770, https://doi.org/10.3389/fevo.2021.783770, 2022.

Riebe, C. S. and Granger, D. E.: Quantifying effects of deep and near-surface chemical erosion on cosmogenic nuclides in soils, saprolite, and sediment, Earth Surface Processes and Landforms, 38, 523–533, https://doi.org/10.1002/esp.3339, 2013.

Riebe, C. S., Kirchner, J. W., Granger, D. E., and Finkel, R. C.: Erosional equilibrium and disequilibrium in the Sierra Nevada, inferred from cosmogenic 26Al and 10Be in alluvial sediment, Geology, 28, 803–806, https://doi.org/10.1130/0091-7613(2000)28<803:EEADIT>2.0.CO;2, 2000.

Roig, J., Tucker, R., Delor, C., Peters, S., and Théveniaut, H.: Carte géologique de la République de Madagascar à 1/1 000 000, Tech. rep., Ministère de Mines, PGRM, Antananarivo, République de Madagascar, 2012.

Salgado, A. A. R., Marent, B. R., Cherem, L. F. S., Bourlès, D., Santos, L. J. C., Braucher, R., and Barreto, H. N.: Denudation and retreat of the Serra do Mar escarpment in southern Brazil derived from in situ-produced 10Be concentration in river sediment, Earth Surface Processes and Landforms, 39, 311–319, https://doi.org/10.1002/esp.3448, 2014.

Schaller, M., von Blanckenburg, F., Hovius, N., and Kubik, P.: Large-scale erosion rates from in situ-produced cosmogenic nuclides in European river sediments, Earth and Planetary Science Letters, 188, 441–458, https://doi.org/10.1016/S0012-821X(01)00320-X, 2001.

Schoonejans, J., Vanacker, V., Opfergelt, S., and Christl, M.: Long-term soil erosion derived from in-situ 10 Be and inventories of meteoric Be in deeply weathered soils in southern Brazil, Chemical Geology, 466, 380–388, https://doi.org/10.1016/j.chemgeo.2017.06.025, 2017.

Schwanghart, W. and Scherler, D.: Short Communication: TopoToolbox 2 - MATLAB-based software for topographic analysis and modeling in Earth surface sciences, Earth Surface Dynamics, 2, 1–7, https://doi.org/10.5194/esurf-2-1-2014, 2014.

Snyder, N. P., Whipple, K. X., Tucker, G. E., and Merritts, D. J.: Landscape response to tectonic forcing: Digital elevation model analysis of stream profiles in the Mendocino triple junction region, northern California, Geological Society of America Bulletin, 112, 1250–1263, https://doi.org/10.1130/0016-7606(2000)112<1250:LRTTFD>2.0.CO;2, 2000.

Song, X.-P., Hansen, M. C., Stehman, S. V., Potapov, P. V., Tyukavina, A., Vermote, E. F., and Townshend, J. R.: Global land change from 1982 to 2016, Nature, 560, 639–643, https://doi.org/10.1038/s41586-018-0411-9, 2018.

Starke, J., Ehlers, T. A., and Schaller, M.: Tectonic and Climatic Controls on the Spatial Distribution of Denudation Rates in Northern Chile (18°S to 23°S) Determined From Cosmogenic Nuclides, Journal of Geophysical Research: Earth Surface, 122, 1949–1971, https://doi.org/10.1002/2016JF004153, 2017.

Stephenson, S. N., White, N. J., Carter, A., Seward, D., Ball, P. W., and Klöcking, M.: Cenozoic Dynamic Topography of Madagascar, Geochemistry, Geophysics, Geosystems, 22, e2020GC009 624, https://doi.org/10.1029/2020GC009624, 2021.

Tucker, R., Roig, J., Moine, B., Delor, C., and Peters, S.: A geological synthesis of the Precambrian shield in Madagascar, Journal of African Earth Sciences, 94, 9–30, https://doi.org/10.1016/j.jafrearsci.2014.02.001, 2014.

Tyson, P.: Madagascar: The Eight Continent. Life, death and discovery in a lost world, Bradt Travel Guides, 2013.

Vanacker, V., von Blanckenburg, F., Govers, G., Molina, A., Poesen, J., Deckers, J., and Kubik, P.: Restoring dense vegetation can slow mountain erosion to near natural benchmark levels, Geology, 35, 303–306, https://doi.org/10.1130/G23109A.1, 2007a.

Vanacker, V., von Blanckenburg, F., Hewawasam, T., and Kubik, P. W.: Constraining landscape development of the Sri Lankan escarpment with cosmogenic nuclides in river sediment, Earth and Planetary Science Letters, 253, 402–414, https://doi.org/10.1016/j.epsl.2006.11.003, 2007b.

Vanacker, V., von Blanckenburg, F., Govers, G., Molina, A., Campforts, B., and Kubik, P. W.: Transient river response, captured by channel steepness and its concavity, Geomorphology, 228, 234–243, https://doi.org/10.1016/j.geomorph.2014.09.013, 2015.

Voarintsoa, N. R. G., Cox, R., Razanatseheno, M. O. M., and Rakotondrazafy, A. F. M.: Relation between bedrock geology, topography and lavaka distribution in Madagascar, South African Journal of Geology, 115, 225–250, https://doi.org/10.2113/gssajg.115.225, 2012.

von Blanckenburg, F.: Cosmogenic nuclide evidence for low weathering and denudation in the wet, tropical highlands of Sri Lanka, Journal of Geophysical Research, 109, F03 008, https://doi.org/10.1029/2003jf000049, 2004.

von Blanckenburg, F.: The control mechanisms of erosion and weathering at basin scale from cosmogenic nuclides in river sediment, Earth and Planetary Science Letters, 237, 462–479, https://doi.org/10.1016/j.epsl.2005.06.030, 2005.

Wang, Y.: Erosion rates and landscape evolution of the conjugate margins of Madagascar and India, Ph.D. thesis, ETH Zürich, https://doi.org/10.3929/ethz-b-000476167, 2021.

Wang, Y. and Willett, S. D.: Escarpment retreat rates derived from detrital cosmogenic nuclide concentrations, Earth Surface Dynamics, 9, 1301–1322, https://doi.org/10.5194/esurf-9-1301-2021, 2021.

Wang, Y., Willett, S. D., Wu, D., Haghipour, N., and Christl, M.: Retreat of the Great Escarpment of Madagascar From Geomorphic Analysis and Cosmogenic 10Be Concentrations, Geochemistry, Geophysics, Geosystems, 22, e2021GC009 979, https://doi.org/10.1029/2021GC009979, 2021.

Whipple, K. X.: Bedrock rivers and the geomorphology of active orogens, Annual Review of Earth and Planetary Sciences, 32, 151–185, https://doi.org/10.1146/annurev.earth.32.101802.120356, 2004.

Whipple, K. X. and Tucker, G. E.: Dynamics of the stream-power river incision model: Implications for height limits of mountain ranges, landscape response timescales, and research needs, Journal of Geophysical Research: Solid Earth, 104, 17 661–17 674, https://doi.org/10.1029/1999JB900120, 1999.

Winkler, K., Fuchs, R., Rounsevell, M., and Herold, M.: Global land use changes are four times greater than previously estimated, Nature Communications, 12, 2501, https://doi.org/10.1038/s41467-021-22702-2, 2021.

Wittmann, H. and von Blanckenburg, F.: Cosmogenic nuclide budgeting of floodplain sediment transfer, Geomorphology, 109, 246–256, https://doi.org/10.1016/j.geomorph.2009.03.006, 2009.

Wobus, C., Whipple, K. X., Kirby, E., Snyder, N., Johnson, J., Spyropolou, K., Crosby, B., and Sheehan, D.: Tectonics from topography: Procedures, promise, and pitfalls, in: Tectonics, Climate, and Landscape Evolution, vol. 398, pp. 55–74, Geological Society of America, https://doi.org/10.1130/2006.2398(04), 2006.

Yanites, B. J., Tucker, G. E., and Anderson, R. S.: Numerical and analytical models of cosmogenic radionuclide dynamics in landslide-dominated drainage basins, Journal of Geophysical Research: Earth Surface, 114, https://doi.org/10.1029/2008JF001088, 2009.

Zaprowski, B. J., Pazzaglia, F. J., and Evenson, E. B.: Climatic influences on profile concavity and river incision, Journal of Geophysical Research: Earth Surface, 110, F03 004, https://doi.org/10.1029/2004JF000138, 2005.

7 Figures

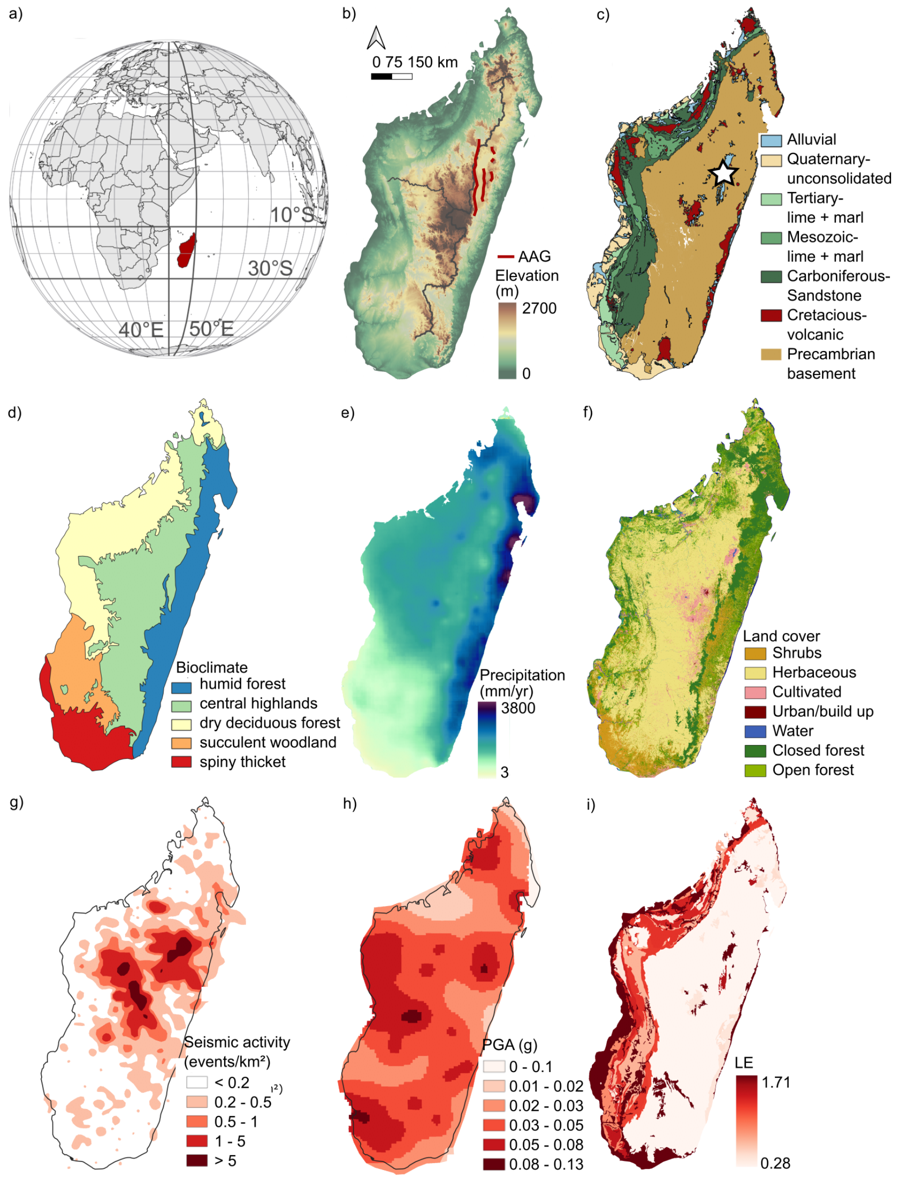

Figure 1: **Spatial variations of environmental variables in Madagascar.** a) Madagascar spans 13° of latitude (12 - 25°S) and is located between ca. 40 and 50°E. b) Elevation from 30 m SRTM (Farr et al., 2007) with indication of the Alaotra Ankay Graben (AAG) and simplified major faults in red from Kusky et al. (2010). The main water divides are indicated in black. c) Simplified geology based on Roig et al. (2012) and Tucker et al. (2014). The star indicates the location of the Ranofotsy catchment. d) Simplified bioclimatic regions from Cornet (1974) and Crowley (2010). e) Average yearly precipitation from CHIRPS 1981-2021 (Funk et al., 2014). f) Main current land cover classes from the Copernicus global land cover map (Buchhorn et al., 2020). g) Seismic activity expressed as the number of seismic events per km² (Cox et al., 2010). h) Peak ground acceleration (PGA) from the Sub-Saharan Africa (SSA) Earthquake Model (Poggi et al., 2017). i) Calculated lithological erodibility (LE) from the lithological map of Roig et al. (2012).

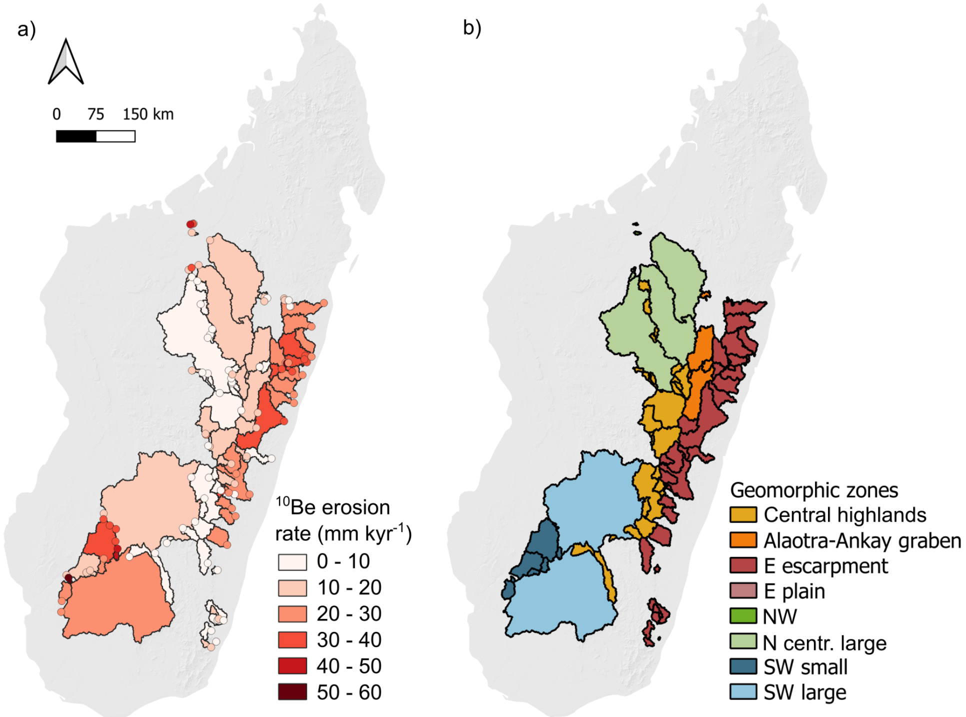

Figure 2: **Maps of ^{10}Be erosion rates and regions.** a) ^{10}Be erosion rates (mm kyr^{-1}) for all sampled catchments. Sampling locations are indicated by the dots, which are also colored for ^{10}Be erosion rate (Table S1). b) Division of the dataset into different regions, with separate categories for the very large (> 10 000 km²) catchments: i) central highlands (n = 27), ii) Alaotra-Ankay graben (AAG) (n = 12), iii) eastern escarpment (n = 32), iv) eastern plain (n = 1), v) northwest (n = 5), vi) north-central large (n = 4), vii) southwest small (n = 11), and viii) southwest large (n = 2). For visualization of the different data sources, larger scale maps and nested catchment structure we refer to Figure S1, S2 and S3 and Table S1.

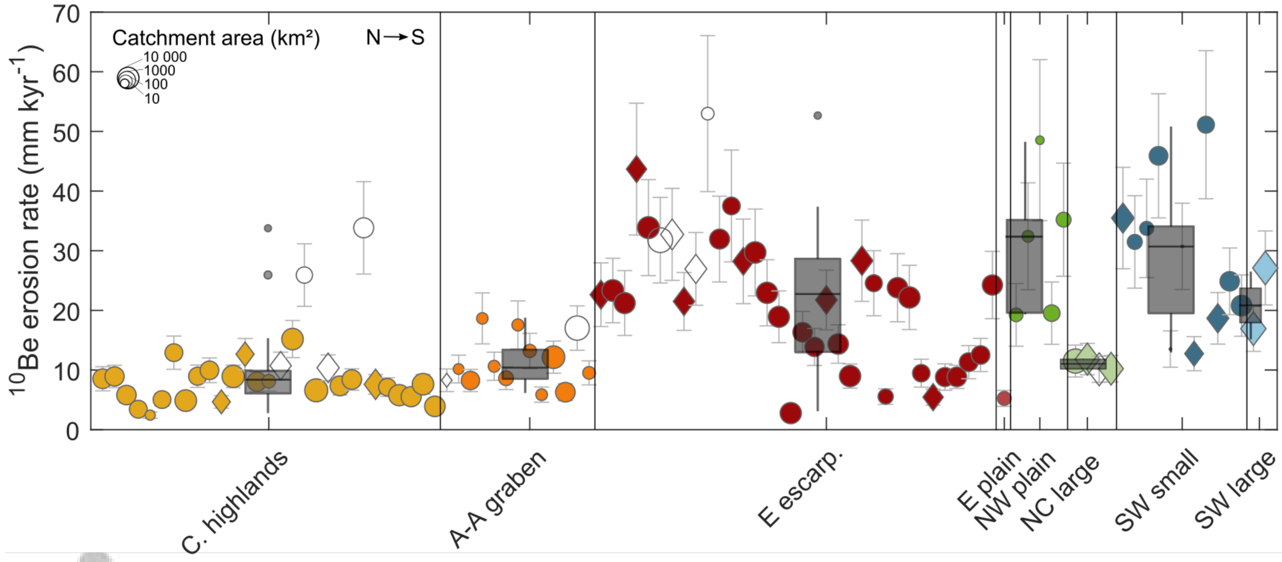

Figure 3: **^{10}Be erosion rates per region.** ^{10}Be erosion rates organized from north to south for the different regions. Marker size represents the catchment area. Boxplots are included for regions that contain sufficient sampled catchments. Hollow dots represent outliers (id = 30, 32, 37, indicated by grey boxplot dots) and catchments in the east that encompass more than one region (id = 94, 95) and are not included in statistical analysis. Filled diamonds represent sub-catchments > 20% of the main basin for which effective erosion rates were calculated and used in further analysis. Hollow diamonds indicate sub-catchments < 20% of the main catchment area and are excluded from further statistical analysis (only the main catchment is used in this case). See Figure S2 and S3 and Table S1 for used nomenclature and nested-basin structure.

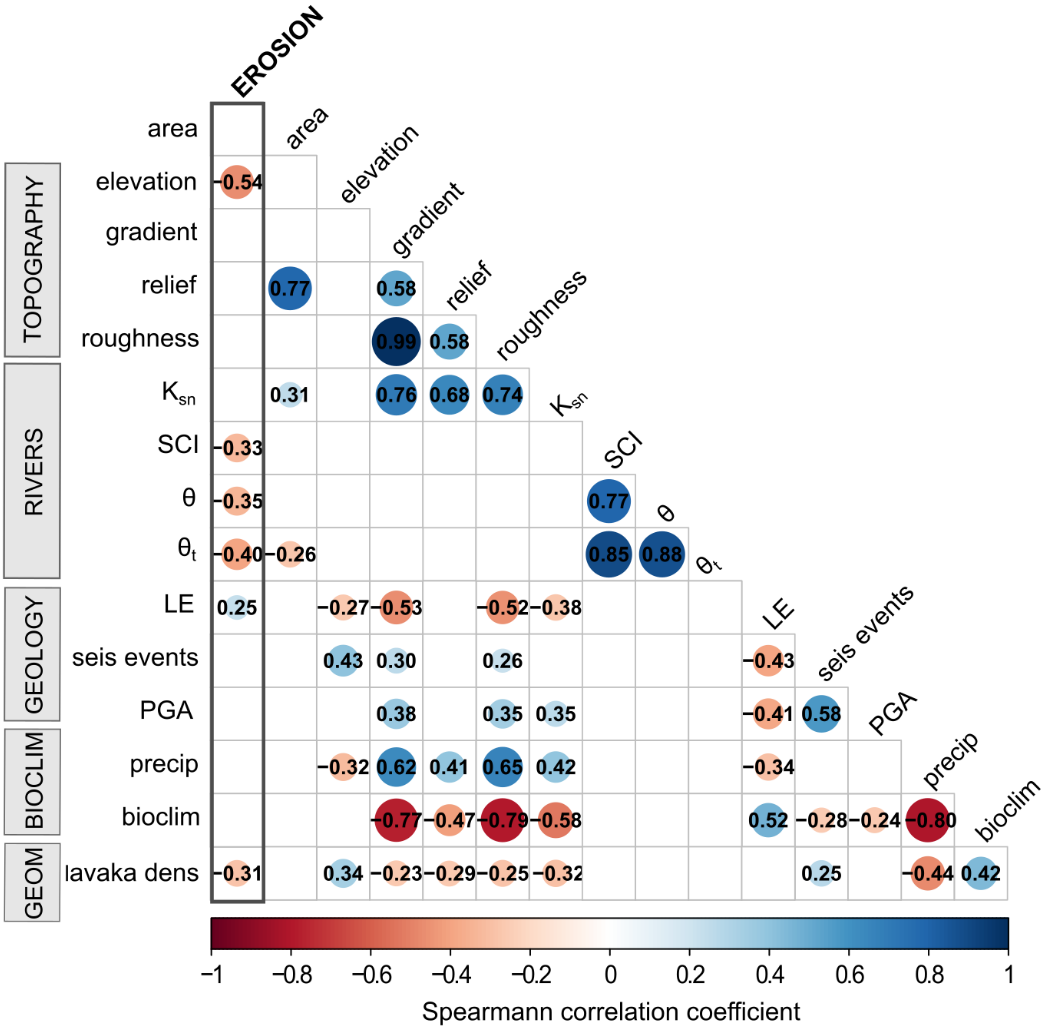

Figure 4: **Spearman rank correlation coefficients.** Spearman rank correlation coefficients between the ^{10}Be erosion rates and fifteen environmental variables when considering the full dataset (n = 88). These variables include catchment area, averaged topographic metrics (mean catchment elevation, slope gradient, relief and roughness), river metrics (normalized river steepness (k_{sn}), stream concavity index (SCI), stream concavity (θ) for all and trunk stream (θ_t)), geological variables (lithological erodibility (LE), number of seismic events and peak ground acceleration (PGA)), bioclimatic variables (average annual precipitation and bioclimatic region), and lavaka density as a geomorphological factor. The color scale and dot-size indicate the strength (bigger dots stronger correlation) and direction (red for negative and blue for positive) of the correlation. Only significant correlations (p-value < 0.05) are plotted.

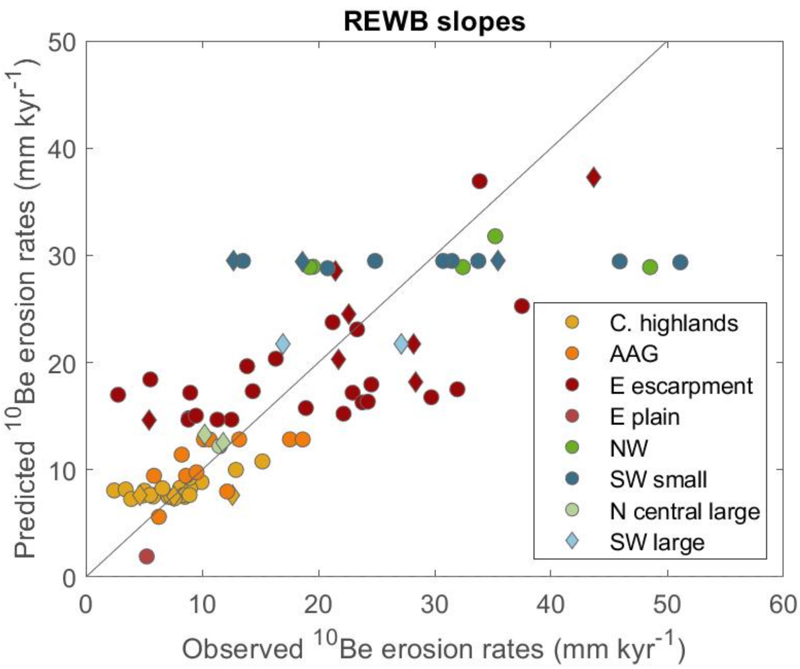

Figure 5: **Observed vs. predicted ^{10}Be erosion rates.** Modelled vs. observed ^{10}Be erosion rates when applying the REWB slopes model (Table 3). The different colors indicate the regions. The line indicates a 1:1 relationship. Dots represent the sampled sub-basins, diamonds indicate the effective erosion rates calculated for the sub-catchments with area > 20% of the parent basin (see also Figure S2, S3 and Table S1).

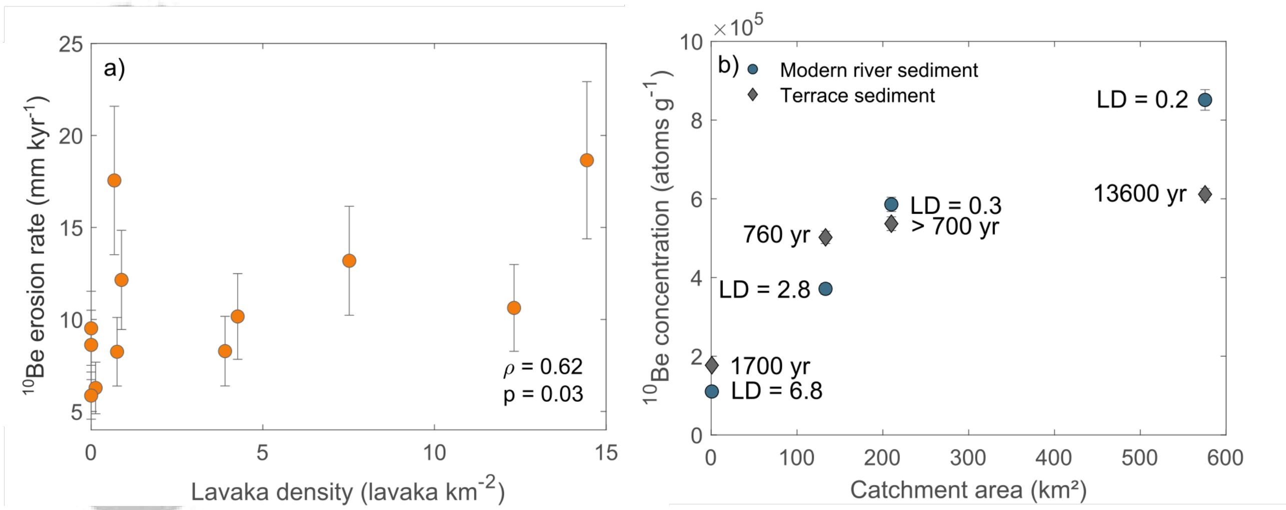

Figure 6: **Impact of lavaka on ^{10}Be concentrations and erosion rates.** a) ^{10}Be erosion rates increase with increasing lavaka density in the Alaotra-Ankay graben region (ρ = 0.62, p = 0.03). b) Comparison of ^{10}Be concentrations measured in modern river sediment and in ^{14}C dated terrace sediments. The age of the terrace sediments is indicated next to the terrace concentrations. Lavaka densities (LD in lavaka per km²) are indicated next to the modern river sediment concentrations.

8 Tables

Table 1: **Factor loadings.** Factor loadings for ^{10}Be erosion rates and the different environmental variables when considering the full dataset (n = 88). Factors loadings above 0.3 are in bold to indicate the main components of the specific factors.

		Factor 1	Factor 2	Factor 3	Factor 4
	erosion	-0.17	**-0.34**	-0.16	0.04
	area	-0.11	-0.10	-0.02	**0.72**
TOPO	elevation	0.13	0.06	0.27	-0.01
	gradient	**0.97**	0.08	0.22	0.02
	relief	**0.57**	0.02	-0.15	**0.81**
	roughness	**0.98**	0.08	0.20	0.02
RIVER	k_{sn}	**0.74**	-0.01	-0.04	0.20
	SCI	0.09	**0.92**	-0.13	0.05
	θ	-0.07	**0.87**	0.03	0.01
	θ_t	-0.06	**0.97**	0.03	-0.18
GEOL	LE	**-0.74**	-0.08	-0.28	-0.06
	seis events	0.02	0.00	**0.91**	0.00
	PGA	0.21	0.02	**0.69**	0.10
BIO	precip	**0.69**	-0.02	-0.04	-0.04
	bioclim	**-0.82**	-0.04	-0.14	0.06
GEOM	lavaka dens	-0.04	-0.03	**0.59**	-0.18

Table 2: **Stepwise linear regressions.** Stepwise linear regression analysis results for the full dataset and the different regions separately. Adjusted R² and AIC for each additional included variables are displayed. θ is the stream concavity, LE the lithological erodibility, and SCI the stream concavity index.

	Step	Coefficient	R²	AIC
Full dataset (n = 88)				
intercept	0	29.11		
elevation	1	-0.01	0.28	652.40
θ	2	-11.53	0.39	639.16
LE	3	6.72	0.43	633.61
Central highlands (n = 25)				
intercept	0	5.81		
seis events	1	2.37	0.41	118.27
AAG (n = 11)				
intercept	0	9.39		
lavaka density	1	0.43	0.23	635
E escarpment (n = 30)				
intercept	0	91.71		
seismic events	1	7.82	0.39	213
LE	2	-138.24	0.44	211
θ_t	3	-15.71	0.52	208
elevation	4	-0.01	0.54	207
precipitation	5	-0.01	0.55	207
SW small (n = 11)				
intercept	0	89.49	0.00	
LE	1	-46.83	0.23	876

Table 3: **RE(WB) model results.** Results of the five models that were applied to the full dataset (n = 88): i) Fixed multiple linear regression, random effects with varying ii) intercept and iii) intercept and regression slope for the different regions, and random within between (REWB) models that allow varying iv) intercept and v) intercept and regression slope for the different regions. Only variables that significantly ($p < 0.05$) explain variations in ^{10}Be erosion rates are included in the model. The coefficients of the fixed effects are displayed together with the variance (σ^2) of the random effects. n indicates the number of regions or observations. The marginal R^2 considers only the variance explained by the fixed effects, whereas the conditional R^2 takes both the fixed and random variance into account. The Akaike Information Criteria (AIC) determines the performance of a model where a lower value indicates a better model (Akaike, 1987).

	Fixed	**Random intercept**	**Random slopes**	**REWB intercept**	**REWB slopes**
FIXED EFFECTS					
(Intercept)	27.43	16.68	24.00	17.53	36.78
elevation	-0.01		-0.01		
θ	-11.79				
LE	5.98				
θ_t		-5.79			
seis events		3.32			
θ - within				-5.47	
seis events - within				3.87	
SCI - between					-61.28
seis events - between					-17.52
lavaka dens - between					17.26
RANDOM EFFECTS					
Residual σ^2	56.13	47.17	56.07	50.68	53.11
σ^2 geo region		135.24	64.51	81.05	31.12
σ^2 seis events			23.92		18.37[a]
σ^2 SCI			114.66		
n regions		8	8	8	8
n observations	88	88	88	88	88
Marginal R^2	0.40	0.11	0.11	0.09	0.44
Conditional R^2	0.38	0.74	0.62	0.63	0.73
AIC	642	624	641	621	612

[a] within-effect